Simulation of Hydrogen Release from a High-Pressure Chamber Considering Real Gas Effects

Kaveh Mohamed

A Thesis

in

The Department

of

Mechanical and Industrial Engineering

Presented in Partial Fulfillment of the Requirements
for the Degree of Master of Applied Science (Mechanical Engineering) at
Concordia University
Montreal, Quebec, Canada

April 2004

Your file Votre référence
ISBN: 0-612-91086-5
Our file Notre référence
ISBN: 0-612-91086-5

ABSTRACT

SIMULATION OF HYDROGEN RELEASE FROM A HIGH-PRESSURE CHAMBER CONSIDERING REAL GAS EFFECTS

Kaveh Mohamed

Hydrogen release from a high-pressure chamber is modeled in this thesis. Two approaches are developed to investigate the real gas effects at high pressures. In the first method, an analytical model is developed to simulate time histories of stagnation properties of hydrogen inside the chamber as well as sonic properties of hydrogen at the orifice. Thermodynamic relations describing the specific heats, internal energy, and speed of sound, are derived based on Beattie-Bridgeman state equation. In the second approach, a 3-D unstructured tetrahedral finite volume Euler solver is applied to numerically simulate the hydrogen release. The solver is modified to take into account the real gas effects. Modifications required to calculate the real gas Jacobian matrices and eigenvectors as well as to obtain the Roe's averaged convective fluxes are described. Real gas effect is also modeled by the same state equation. Numerical and analytical results are compared for ideal and real gas conditions. An excellent agreement is reported.

ACKNOWLEDGMENTS

I wish to thank my supervisor, Professor Marius Paraschivoiu, for all his support and guidance throughout the research.

TABLE OF CONTENTS

LIST OF FIGURES

LIST OF TABLES

NOTATIONS

a	Speed of sound
A_n	Throat surface area
A_o	Constant of Beattie-Bridgeman EOS
b	Constant of Beattie-Bridgeman EOS
B_o	Constant of Beattie-Bridgeman EOS
c	Constant of Beattie-Bridgeman EOS
C_υ	Specific heat of the real gas at constant volume
C_P	Specific heat of the real gas at constant pressure
$\widetilde{C}_\upsilon$	Specific heat of the ideal gas at constant volume
$\widetilde{C}_P$	Specific heat of the ideal gas at constant pressure
d	Differential change
E	Total internal energy
f	State equation
h	Enthalpy
H	Total enthalpy
i	Internal energy
l	Auxiliary variable
M	Molecular mass of hydrogen
n_x	x-component of unit normal vector $\vec{n}$
n_y	y-component of unit normal vector $\vec{n}$
n_z	z-component of unit normal vector $\vec{n}$
m	Auxiliary variable
o	Auxiliary variable
P	Pressure
R	Gas constant
s	Entropy
ΔS	Surface area of the control volume's boundary
u	x-component of velocity
v	y-component of velocity
w	z-component of velocity
V	Magnitude of velocity vector
υ	Specific volume
υ°	Specific heat at temperature T and pressure of 10^5 Pa

t	Time
Δt	Time step
T	Temperature
Z	Compressibility factor

Greek Letters

α	Constant of Beattie-Bridgeman EOS
δ	Small change
Ψ	Total volume of the chamber
ε	Auxiliary variable
φ	State equation
γ	Ratio of specific heats for ideal gas condition
λ	Eigenvector
ρ	Density
τ_j^c	Control volume j
$\left\|\tau_j^c\right\|$	Volume of the control volume j
$\delta\tau_j^c$	Boundary surfaces of control volume j
Γ	Residual

Vectors and Matrices

$[A]$	Conservative Jacobian in x-direction
$[B]$	Conservative Jacobian in y-direction
$[C]$	Conservative Jacobian in z-direction
$[\widetilde{A}]$	Primitive Jacobian in x-direction
$[\widetilde{B}]$	Primitive Jacobian in y-direction
$[\widetilde{C}]$	Primitive Jacobian in z-direction
$\vec{\vec{F}}$	Conservative fluxes in all directions
$\vec{g}$	Conservative flux vector in y-direction
$\vec{h}$	Conservative flux vector in z-direction
$\vec{\vec{I}}$	Unit 5×5 matrix
$[K]$	Conservative Jacobian in an arbitrary direction $\vec{n}$
$[\widetilde{K}]$	Primitive Jacobian in an arbitrary direction $\vec{n}$

$\vec{k}$	Conservative flux vector in x-direction
l_j	Components of the left eigenvector
$[\Lambda]$	Diagonal matrix of eigenvalues
$[L]$	Left eigenvector matrix
r_j	Components of the right eigenvector
$[L]$	Right eigenvector matrix
$[M]$	Conservative to primitive transformation matrix
$[M^{-1}]$	Primitive to conservative transformation matrix
$\vec{n}$	Unit normal vector to boundary surfaces of control volumes
$\vec{Q}$	Vector of Primitive variables
$\vec{U}$	Vector of Conservative variables
$\vec{V}$	Velocity vector

Superscripts

n	Time step
~	Primitive values
^	Roe's averaged values
T	Transpose

Subscripts

i	Partial derivative with respect to internal energy
j	Mesh point location
υ	Partial derivative with respect to specific volume
ρ	Partial derivative with respect to density
n	Property at the throat
t	Total or stagnation property
T	Partial derivative with respect to temperature

Abbreviations

CFL	Courant-Friedrichs and Lewy number
EOS	Equation of state

Chapter 1

INTRODUCTION

1.1 Hydrogen Scope as a Fuel

Today's formidable environmental problems and the limitation of hydrocarbon fuel resources oblige industries to substitute crude oil products, natural gas and coal with a clean and recyclable energy source. Hydrogen has some advantageous features and can be considered as a potential energy candidate in many systems. In particular, hydrogen can be supplied as a motor vehicle fuel. It has an advantage that it undergoes a very efficient combustion with air and produces low amount of pollution, especially when it is used in a fuel cell to generate electricity.

The problem with using hydrogen as a fuel is its storage. Compared to natural gas, hydrogen has smaller energy content per mole, and less moles of hydrogen can be stored in a given volume at the same pressure; e.g., standard Compressed Natural Gas (CNG) cylinders* filled with natural gas and hydrogen at a same pressure of 20.78 MPa contain energy amounts that are respectively equivalent to 9.44 l and 1.87 l of gasoline, [1]. Real gas behavior in hydrogen is associated with a reduction in the hydrogen tendency to occupy smaller volumes at higher pressures. The deviation from the ideal gas law is quantified by the compressibility factor. It is defined as,

$$Z = \frac{pv}{RT}. \tag{1.1}$$

* Luxfer N250W-30 filament wound aluminum cylinder (113 cm × 22.3 cm OD, 23.4 kg).

In an ideal gas, Z is always equal to one. The compressibility factor of hydrogen at 300° K is plotted versus pressure in fig. 1.1, where densities are calculated based on the Beattie-Bridgeman state equation. The compressibility factor monotonically increases to values well above unity (ideal value) at high pressures. Therefore, the volume required for storing a specific mass of hydrogen at a relatively high pressure is much larger than the volume the ideal gas law predicts; e.g., at a pressure of 30 MPa the volume is 20% larger than the prediction of the ideal gas law. For natural gas, on the contrary, the compressibility factor decreases at first and reaches a minimum value as the pressure rises to above atmospheric values; Z is equal to 0.75 at 20 MPa, [1]. Further pressure increases result in a monotonic growth of the compressibility factor. The difference in compressibility factor implies that hydrogen should be held at higher pressures compared to natural gas in order to store a reasonable amount of fuel in a vehicle.

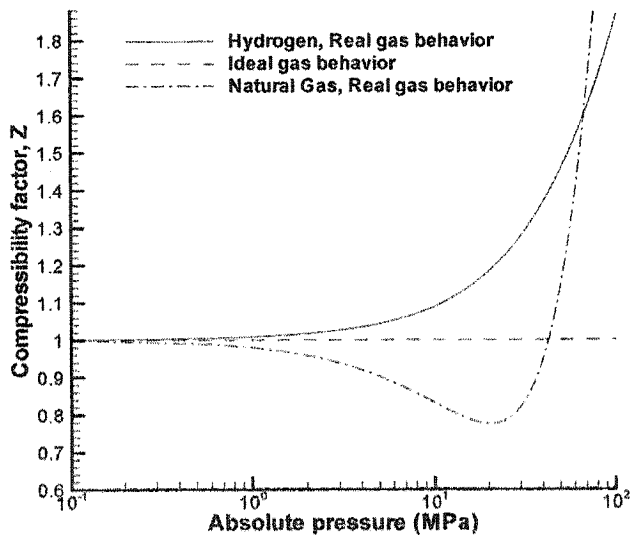

Fig. 1.1: *Compressibility factors of hydrogen and natural gas at 300° K, the real gas values for hydrogen are obtained from Beattie-Bridgman EOS.*

Hydrogen can be stored using different systems such as compressed gas cylinders, metal hydrides, glass micro-spheres, cryogenic liquid and ammonia. These systems are investigated in terms of their volumes, weights and energy contents in [2]. Among them, gaseous hydrogen at high pressures is one form of storage that is seriously considered for automotive applications. Hydrogen is presently stored at pressures up to 43.8 MPa and can be delivered to vehicle tanks at settled pressures of 35.0 MPa. Ground storage at 87.5 MPa for 70.0 MPa vehicle tank fills is being considered in the future and may become a standard for transportation applications.

For safety issues, it is important to determine how the gas is released in case of failure. The worst most probable failure is the separation of a fitting in a high-pressure tube or pipe, which would result in a sudden release of hydrogen. The release of hydrogen into the air yields a detonable cloud. The mixture of hydrogen and air is considered explosive if the volumetric concentration of hydrogen lies between 4.0% and 77.0%, [3]. Important safety considerations entail high precision models to describe the hydrogen release from a high-pressure container. This crucial accuracy cannot be obtained unless an appropriate real gas law is applied in development of analytical and numerical models.

1.2 Modeling of the Hydrogen Release: Objectives

In this study, unsteady release of hydrogen from a high-pressure chamber is analytically and numerically simulated. Beattie-Bridgeman equation of state (EOS) is substituted for the ideal gas law to take into account the real gas effects at high pressures. The chamber considered as a model problem contains hydrogen at an initial pressure and temperature of 34.5 MPa and 300° K. The inside gas adiabatically exits the chamber through an orifice to

the atmosphere. We investigate the real gas effects on different thermodynamic properties of the gas inside the chamber and the gas crossing the throat. We calculate the mass flow rate of hydrogen exiting the chamber and the exit velocity. These data can be used as boundary conditions in later studies to investigate the diffusion of hydrogen into the atmospheric air in order to minimize the risk of detonation, [3].

This thesis was initially started by an existing need from industry to simulate hydrogen flow at high pressures. The problem is tackled by developing an analytical model for the sample case described in the last paragraph and then bringing forth a more sophisticated numerical simulation tool for real gas flows. The predictions of the analytical model are used to validate the results of the numerical simulation.

User-friendly menus and robustness of commercial CFD softwares make them the first choice in industrial simulation applications. Therefore, it was intended, at first, to use FLUENT 6 to perform the real gas simulations. Since FLUENT 6 does not have any specific module to deal with the real gas effects for hydrogen [4], the plan was to write user defined adjust functions (UDF) and to run them at each FLUENT's time iteration. The UDF's were supposed to do the required corrections on thermodynamic properties as well as to extract primitive variables from recently calculated conservative variables, which are direct solutions of the system of Euler equations. The problem of this approach is that FLUENT transforms the system of Euler equations, which is originally in terms of the conservative quantities, into a new form based on the primitive variables. The transformation matrix is completely dependent on the ideal gas law. Therefore, FLUENT restricts us to ideal gases as we cannot access the transformation matrix using any UDF's.

The next alternative was the extension of an existing in-house 3-D finite volume Euler solver. This code uses an implicit first-order in time and second-order in space scheme. Conservative fluxes are calculated using Roe's averaging method. To predict the real gas behavior, new flux Jacobians, conservative-primitive transformation matrices, left and right eigenvector matrices are derived and applied to the code according to the real gas state equation. The definitions of the averaged variables are modified in order to maintain unique properties of Roe's method for real gas conditions.

1.3 Review of Techniques for Real Gas Simulations

Several extensions of Roe's averaging method to real gas flows exist in the literature. Most of the work deals with the simulation of flows at high Mach numbers and high temperatures, where the goal is to compute hypersonic flows in atmosphere reentries or suborbital flights. The extensions of Roe's scheme to the real gas flow can be classified into two general categories. In the first category an equivalent γ (ratio of specific heats) is defined and appropriate assumptions are made to keep the conformity with the perfect gas equation of state. Grossman et al. [5, 6] applied this technique to simulate high temperature and high Mach number flows in 1, 2 and 3-D problems. The same approach is used in [7, 29] to develop a parabolized Navier-Stokes code to compute the three-dimensional hypersonic external flow of the equilibrium air around various geometries.

A more thorough approach is utilized in the second category, where averaging procedures are defined for pressure derivatives that appear in the Jacobian matrix. These definitions are not unique. In addition, different thermodynamic properties may be selected as independent variables in the state equation that explicitly describes the pressure. Each

distinct selection requires specific definitions of the corresponding pressure derivatives; e.g., if the density and the internal energy are selected as independent variables, averaged values for derivatives of the pressure with respect to the density and the internal energy should be defined. Different averaging relations have been presented in the literature. Glaister [8] applied this method to numerically simulate the standard 1-D shock reflection problem. In his work, pressure is given as a function of the density and the internal energy in the state equation. Vinokur et al. [9] and Montagne et al. [28] presented different averaging definitions for pressure derivatives using the same independent variables as those in Glaister's work. The averaging method developed by Liou et al. in [10] is applied to simulate 1-D unsteady shock tube and steady nozzle flows. The state equation they used explicitly describes the pressure in terms of the density and internal energy with 20 basis functions. An extension of the Roe's averaging method to a mixture of perfect gases that are in thermal and chemical equilibrium condition is introduced and applied to solve the 2-D hypersonic flow around a simple ellipse in [11]. The density and the enthalpy are selected as independent variables in the state equation in [12] and the corresponding generalized definitions of Roe's averaged values are used to simulate a 1-D two-phase flow in a smooth pipe. Buffard et al. [13] developed an approximate Riemann solver to compute Euler equations in terms of non-conservative variables using the real gas state equation. They modified an alternative to the Roe's scheme called VFRoe in order to solve for non-conservative variables. A review of several generalizations of the Roe's scheme is given in [14]. Numerical performances of these methods are compared together by simulating the steady hypersonic flow around a 2-D blunt body.

In this thesis, the method introduced by Glaister is applied to modify the convective fluxes in a 3-D finite volume Euler solver. Hydrogen release from a high-pressure chamber is simulated as a sample problem. The original aspect of this work is the development of 3-D Jacobians, transformation matrices, and eigenvector matrices based on the Beattie-Bridgeman EOS.

Analytical models describing the isentropic expansion of a real gas from a high-pressure plenum are introduced in [15, 16]. Johnson [15] applied these models to tabulate sonic and stagnation properties of nitrogen and helium at pressures up to 30 MPa. In this thesis, the same algorithm is applied to a different EOS (Beattie-Bridgeman EOS) to derive the thermodynamic relations and develop an analytical model.

1.4 Thesis Outline

The rest of the thesis is as follows. Chapter 2 is devoted to the development of an analytical model to describe the real gas release from a high-pressure chamber. Thermodynamic relations are derived to calculate specific heats, internal energy, sound velocity and isentropic expansion of a real gas based on the Beattie-Bridgeman state equation. A numerical scheme is introduced, in Chapter 3, to simulate the real gas flow. The flux Jacobian, transformation matrices, left and right eigenvector matrices as well as the definitions of the Roe's averaged variables for the real gas are detailed in this chapter. Results of the analytical and numerical simulations are investigated and compared to the ideal gas predictions in Chapter 4. Conclusions and recommendations for future work are brought forth in Chapter 5.

Chapter 2

ANALYTICAL MODEL

In this chapter, an analytical model is developed to describe the hydrogen release from a high-pressure chamber, whereby time histories of the stagnation and sonic properties are calculated. Thermodynamic relations are derived based on a reference EOS in which the pressure is explicitly given in terms of two independent thermodynamic properties. The relations are used to calculate the specific heats, the internal energy, the speed of sound, and the isentropic derivatives in terms of the independent thermodynamic properties.

2.1 Definition of the Problem

A chamber is assumed to store hydrogen initially at a high pressure. Hydrogen exits the chamber through an orifice to atmospheric air. No heat transfer occurs between the gas inside the chamber and its surrounding during the release. A control-volume approach is applied in this section to develop a model that describes the hydrogen release. Time histories of thermodynamic properties are sought at two locations: inside the chamber where stagnation properties are calculated, and at the orifice where sonic properties are obtained. The schematic diagram of the control volume of the problem is shown in fig. 2.1.

The thermodynamic behavior of a gas at high pressures deviates from what is described by the ideal gas law, fig 1.1. In order to take into account this deviation, the analytical model developed in this chapter is based on a real gas equation of state. Using the real gas EOS, thermodynamic relations are derived to relate the specific heats, the internal energy,

the speed of sound, and isentropic derivatives to the independent thermodynamic properties.

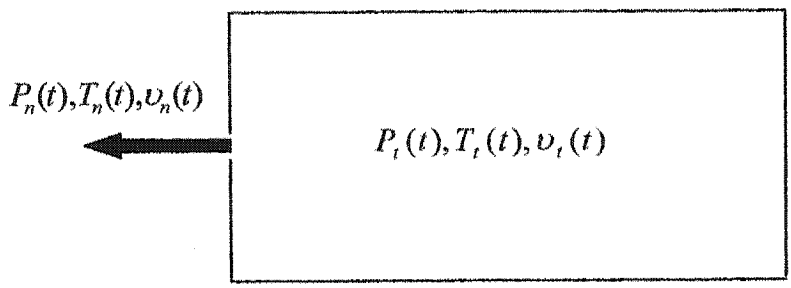

Fig. 2.1: *Schematic diagram of the control volume for analytical model.*

2.2 Assumptions

The following assumptions have been made to simulate the gas release from a high-pressure chamber:

1. Thermodynamic properties are distributed uniformly throughout the chamber;
2. The hydrogen release is simulated at adiabatic conditions where no heat transfer occurs between the gas inside the chamber and its surrounding container;
3. The orifice is at the critical condition (i.e., the velocity of the gas at the orifice is equal to the local speed of sound);
4. The expansion of hydrogen from the stagnation state at the chamber to the critical state at the orifice takes place at a small region near the orifice, and it is modeled by a quasi one-dimensional isentropic flow;
5. Hydrogen is assumed to exist in gaseous phase through the whole chamber;

6. The real gas behavior is modeled by the Beattie-Bridgeman state equation, equation (2.1), which is considered as the reference equation in this thesis. All required constants of the equation, $A_\circ$, $B_\circ$, α, b, and c are listed in table 1.1.

$$P = f(T,\upsilon) = \frac{RT}{\upsilon} + \left(\frac{-cR}{T^2} + B_\circ RT - A_\circ\right)\frac{1}{\upsilon^2} + \left(-\frac{B_\circ cR}{T^2} - B_\circ bRT + \alpha A_\circ\right)\frac{1}{\upsilon^3} + \frac{B_\circ bcR}{T^2}\frac{1}{\upsilon^4}. \quad (2.1)$$

Although the first and fourth assumptions seem contrary to each other, they will give reasonable results for a large high-pressure chamber with a small orifice, [17]. If the total time of the gas release is not a concern, the third assumption is acceptable. After the flow reaches subsonic speeds at the orifice, pressure, density, and temperature-changes become very small and negligible compared to corresponding values that exist when the flow is sonic at the orifice.

In the following subsections, foregoing assumptions are applied to write the conservations of mass and energy as well as to derive some real gas thermodynamic relations.

Table 2.1: *Constants of the Beattie-Bridgeman equation of state for hydrogen.*

$A_\circ$	$10^{+3}\alpha$	$10^{+2}B_\circ$	$10^{+2}b$	$10^{-2}c$
4.924	-2.510	1.034	-2.162	2.500

2.3 Conservation Equations

Time derivatives of the stagnation specific volume and stagnation internal energy of the gas inside the chamber can be calculated by balancing the mass and the energy for the control volume shown in fig. 1.1. The conservation of mass is given by:

$$\frac{\partial}{\partial t}\left(\frac{\Psi}{\upsilon_t}\right) = -\frac{a_n A_n}{\upsilon_n}. \tag{2.2}$$

The energy balance can be written as:

$$\frac{\partial}{\partial t}\left(\frac{\Psi i_t}{\upsilon_t}\right) = -\frac{\left(h_n + 0.5a_n^2\right)a_n A_n}{\upsilon_n}. \tag{2.3}$$

Expanding the derivatives on the left hand sides of equations (2.2) and (2.3), we rewrite the above equations as:

$$-\frac{\Psi}{\upsilon_t^2}\frac{\partial \upsilon_t}{\partial t} = -\frac{a_n A_n}{\upsilon_n}, \tag{2.4}$$

$$\frac{\Psi}{\upsilon_t}\frac{\partial i_t}{\partial t} - \frac{\Psi i_t}{\upsilon_t^2}\frac{\partial \upsilon_t}{\partial t} = -\frac{\left(h_n + 0.5a_n^2\right)a_n A_n}{\upsilon_n}. \tag{2.5}$$

After substituting $\frac{\partial \upsilon_t}{\partial t}$ from equation (2.4) into equation (2.5) and rearranging the above equations, final forms of the conservation equations are obtained as:

$$\frac{\partial \upsilon_t}{\partial t} = \frac{\upsilon_t^2}{\Psi}\frac{a_n A_n}{\upsilon_n}, \tag{2.6}$$

$$\frac{\partial i_t}{\partial t} = -\frac{\left(h_n + 0.5a_n^2\right)a_n A_n}{\Psi}\frac{\upsilon_t}{\upsilon_n} + \frac{i_t a_n A_n}{\Psi}\frac{\upsilon_t}{\upsilon_n}. \tag{2.7}$$

Thermodynamic properties of the flow crossing the orifice appear on the right hand sides of conservation equations (2.6) and (2.7). In the following section, relations between dependent and independent thermodynamic properties are defined and then an expression that governs the isentropic expansion or compression is developed.

2.4 Some Real Gas Thermodynamic Relations

In order to keep consistency with the state equation (2.1), temperature and specific volume are selected as independent thermodynamic properties. Speed of sound, specific heats, internal energy and enthalpy are calculated in terms of temperature and specific volume. Mathematically, different relations between dependent and independent properties can be obtained if another form of the state equation is utilized, [15].

For a pure substance, the following relations exist between changes in entropy, temperature, pressure, and specific volume [18]:

$$ds = C_v \frac{dT}{T} + \left(\frac{\partial P}{\partial T}\right)_\upsilon d\upsilon = C_P \frac{dT}{T} - \left(\frac{\partial \upsilon}{\partial T}\right)_P dP. \tag{2.8}$$

In an isentropic process, entropy remains constant and equations (2.8) are reduced to the following forms:

$$\left(\frac{\partial T}{\partial \upsilon}\right)_s = -\frac{T}{C_v}\left(\frac{\partial P}{\partial T}\right)_\upsilon, \tag{2.9}$$

$$\left(\frac{\partial T}{\partial P}\right)_s = \frac{T}{C_P}\left(\frac{\partial \upsilon}{\partial T}\right)_P. \tag{2.10}$$

2.4.1 Specific Heats

The specific heats of hydrogen at constant pressure are tabulated in [19] for the range of temperature between 0° K to 6000° K. The table is given in Appendix A. These values correspond to a reference pressure of 0.1 MPa. Hydrogen behaves like an ideal gas at this reference pressure. These values should be modified at high pressures to allow for the real gas effects.

The following procedure is applied to modify the ideal value of the specific heat and to calculate the corresponding real value at a desired state specified by temperature T and specific volume υ. The first step is to calculate the ideal value of the specific heat, $\tilde{C}_p$, at temperature T and for the reference pressure of 0.1 MPa. This is done by searching through the data given in Appendix A and interpolating between values. The specific heat at constant volume and the specific volume of hydrogen at the reference pressure and temperature T can be obtained from the ideal gas relations as:

$$\tilde{C}_\upsilon(T) = \tilde{C}_P(T) - R, \tag{2.11}$$

$$\upsilon^\circ = \frac{RT}{10^5}. \tag{2.12}$$

In the second step, the value of the specific heat given by equation (2.11) is modified by assuming a constant-temperature process through which the specific volume of hydrogen is changed from υ° to υ. This modification can be formulated as:

$$C_\upsilon(T,\upsilon) = \tilde{C}_\upsilon(T) + \int_{\upsilon^\circ}^{\upsilon} \left(\frac{\partial C_\upsilon}{\partial \upsilon}\right)_T d\upsilon. \tag{2.13}$$

In a pure substance, the derivative of the specific heat with respect to the specific volume for constant temperature is given by, [18]:

$$\left(\frac{\partial C_\upsilon}{\partial \upsilon}\right)_T = T\left(\frac{\partial^2 P}{\partial T^2}\right)_\upsilon. \tag{2.14}$$

After substituting equation (2.14) into equation (2.13), the specific heat at constant volume at temperature T and specific volume υ is written as:

$$C_\upsilon(T,\upsilon) = \tilde{C}_\upsilon(T) + \int_{\upsilon^\circ}^{\upsilon} T\left(\frac{\partial^2 P}{\partial T^2}\right)_\upsilon d\upsilon = \tilde{C}_\upsilon(T) + \int_{\upsilon^\circ}^{\upsilon} T f_{TT}\, d\upsilon. \tag{2.15}$$

The relation between the specific heat at constant volume and the specific heat at constant pressure in a pure substance is given by [18]:

$$C_P(T,\upsilon)-C_\upsilon(T,\upsilon)=-T\left(\frac{\partial \upsilon}{\partial T}\right)_P^2\left(\frac{\partial P}{\partial \upsilon}\right)_T=-T\left(\frac{\partial P}{\partial T}\right)_\upsilon^2\Big/\left(\frac{\partial P}{\partial \upsilon}\right)_T, \tag{2.16}$$

which can be rearranged into the following form to calculate the specific heat at constant pressure:

$$C_P(T,\upsilon)=C_\upsilon(T,\upsilon)-T\frac{f_T^2(T,\upsilon)}{f_\upsilon(T,\upsilon)}. \tag{2.17}$$

2.4.2 Speed of Sound

By definition, the sound velocity in a pure substance is given by [18]:

$$a=\sqrt{\left(\frac{\partial P}{\partial \rho}\right)_s}=\sqrt{-\upsilon^2\left(\frac{\partial P}{\partial \upsilon}\right)_s}=\sqrt{-\upsilon^2\frac{(\partial T/\partial \upsilon)_s}{(\partial T/\partial P)_s}}. \tag{2.18}$$

The isentropic derivatives in equation (2.18) are replaced with their equivalent forms given by equations (2.9) and (2.10). It leads to the following equation:

$$a=\sqrt{\upsilon^2\frac{C_P}{C_\upsilon}\frac{(\partial P/\partial T)_\upsilon}{(\partial \upsilon/\partial T)_P}}=\sqrt{-\upsilon^2\frac{C_P}{C_\upsilon}\left(\frac{\partial P}{\partial \upsilon}\right)_T}, \tag{2.19}$$

which is subsequently represented by:

$$a(T,\upsilon)=\sqrt{-\upsilon^2\frac{C_P}{C_\upsilon}f_\upsilon(T,\upsilon)}. \tag{2.20}$$

2.4.3 Internal Energy

The internal energy of a pure substance is generally a function of its temperature and specific volume. The relation between changes in temperature and specific volume and the corresponding change in internal energy is written as, [18]:

$$di = C_\upsilon dT + \left[T\left(\frac{\partial P}{\partial T}\right)_\upsilon - P \right] d\upsilon. \tag{2.21}$$

The internal energy of hydrogen at temperature T and specific volume υ is obtained by considering two successive processes. The first process occurs at a constant-pressure of 0.1 MPa, during which the temperature of hydrogen increases from 0° K (where the internal energy is zero) to the final temperature of T. Hydrogen is considered as an ideal gas at this pressure; therefore, the bracket in equation (2.21) is always zero during the first process. Using the data given in Appendix A, we can calculate the increase in the internal energy as:

$$\Delta_1 i = \int_0^T \widetilde{C}_\upsilon dT. \tag{2.22}$$

The specific volume of hydrogen at the end of the first process is equal to $\upsilon°$, which is given by equation (2.12). In the second process, the specific volume of hydrogen changes from $\upsilon°$ to the final value of υ while the temperature is kept constant. The corresponding change in the internal energy is calculated from equation (2.21) as:

$$\Delta_2 i = \int_{\upsilon°}^{\upsilon} \left[T\left(\frac{\partial P}{\partial T}\right)_\upsilon - P \right] d\upsilon. \tag{2.23}$$

Combining equations (2.22) and (2.23), we obtain a relation for the internal energy of hydrogen as a real gas,

$$i(T,\upsilon) = \int_0^T \widetilde{C}_v T + \int_{\upsilon°}^{\upsilon} \left[T f_T(T,\upsilon) - f(T,\upsilon) \right] d\upsilon, \tag{2.24}$$

and the enthalpy is given by definition as:

$$h(T,\upsilon) = i(T,\upsilon) + \upsilon f(T,\upsilon). \tag{2.25}$$

2.4.4 Isentropic Expansion

Hydrogen goes through an isentropic expansion from the stagnation state in the chamber to the sonic state at the orifice. Properties of the isentropically expanded flow can be determined by integrating the ordinary differential equation (2.9) with respect to the specific volume.

$$dT = -\frac{Tf_T(T,\upsilon)}{C_\upsilon(T,\upsilon)}d\upsilon. \tag{2.26}$$

Equation (2.26) is integrated from the stagnation state inside the chamber to find thermodynamic states hydrogen goes through during an isentropic expansion. The sonic state of the flow at the throat is the state at which the following balance of energy is satisfied:

$$i(T_t,\upsilon_t)+\upsilon_t f(T_t,\upsilon_t) = i(T_n,\upsilon_n)+\upsilon_n f(T_n,\upsilon_n)+\frac{1}{2}a^2(T_n,\upsilon_n). \tag{2.27}$$

The last two equations are used to uniquely determine sonic properties of hydrogen at the orifice. Analytical expressions for derivatives and integrals are given in table 2.2.

Table 2.2: *Analytical expressions of integrals and derivatives of the state equation.*

f_T	$\frac{R}{\upsilon}+\left(\frac{2cR}{T^3}+B_oR\right)\frac{1}{\upsilon^2}+\left(\frac{2B_ocR}{T^3}-B_obR\right)\frac{1}{\upsilon^3}-\frac{2B_obcR}{T^3}\frac{1}{\upsilon^4}$
f_υ	$-\frac{RT}{\upsilon^2}-\left(\frac{-cR}{T^2}+B_oRT-A_o\right)\frac{2}{\upsilon^3}-\left(-\frac{B_ocR}{T^2}-B_obRT+aA_o\right)\frac{3}{\upsilon^4}-\frac{B_obcR}{T^2}\frac{4}{\upsilon^5}$
$\int_{\upsilon^\circ}^{\upsilon} Tf_{TT}(T,\upsilon)d\upsilon$	$\frac{6cR}{T^3}\left(\frac{1}{\upsilon}-\frac{1}{\upsilon^\circ}\right)+\frac{3B_ocR}{T^3}\left(\frac{1}{\upsilon^2}-\frac{1}{\upsilon^{\circ 2}}\right)-\frac{2B_obcR}{T^3}\left(\frac{1}{\upsilon^3}-\frac{1}{\upsilon^{\circ 3}}\right)$
$\int_{\upsilon^\circ}^{\upsilon}\left[Tf_T(T,\upsilon)-f(T,\upsilon)\right]d\upsilon$	$\left(\frac{3cR}{T^2}+A_o\right)\left(\frac{1}{\upsilon^\circ}-\frac{1}{\upsilon}\right)+\left(\frac{3B_ocR}{T^2}-aA_o\right)\left(\frac{1}{2\upsilon^{\circ 2}}-\frac{1}{2\upsilon^2}\right)-\frac{3B_obcR}{T^2}\left(\frac{1}{3\upsilon^{\circ 3}}-\frac{1}{3\upsilon^3}\right)$
i_T	$\tilde{C}_\upsilon-\frac{6cR}{T^3}\left(\frac{1}{\upsilon^\circ}-\frac{1}{\upsilon}\right)-\frac{6B_ocR}{T^3}\left(\frac{1}{2\upsilon^{\circ 2}}-\frac{1}{2\upsilon^2}\right)+\frac{6B_obcR}{T^3}\left(\frac{1}{3\upsilon^{\circ 3}}-\frac{1}{3\upsilon^3}\right)$
i_υ	$\left(\frac{3cR}{T^2}+A_o\right)\frac{1}{\upsilon^2}+\left(\frac{3B_ocR}{T^2}-aA_o\right)\frac{1}{\upsilon^3}-\frac{3B_obcR}{T^2}\frac{1}{\upsilon^4}$

2.5 Computer Code

A computer program is developed to calculate time histories of stagnation and sonic properties of hydrogen during the release from a high-pressure chamber. It is based on relations developed in Sections 2.3 and 2.4. The program consists of two major steps, isentropic expansion and adiabatic release. The flowchart of the program's algorithm is shown in fig. 2.2. P_{back} is the atmospheric pressure to which hydrogen discharges.

2.5.1 Isentropic Expansion

This step involves the numerical integration of the ordinary differential equation (2.26). The domain of integration consists of all expanded states hydrogen goes through, from the stagnation state inside the chamber to the sonic state at the orifice. The initial condition is determined from the current stagnation state inside the chamber, and the final condition is reached once equality (2.27) is satisfied. After each integration step, equation (2.27) is checked. Its right hand side is evaluated at the most recently computed values of specific volume and temperature. The integration is performed using the first-order Euler method. The integration step is equal to 0.05% of the stagnation specific volume of the gas inside the chamber.

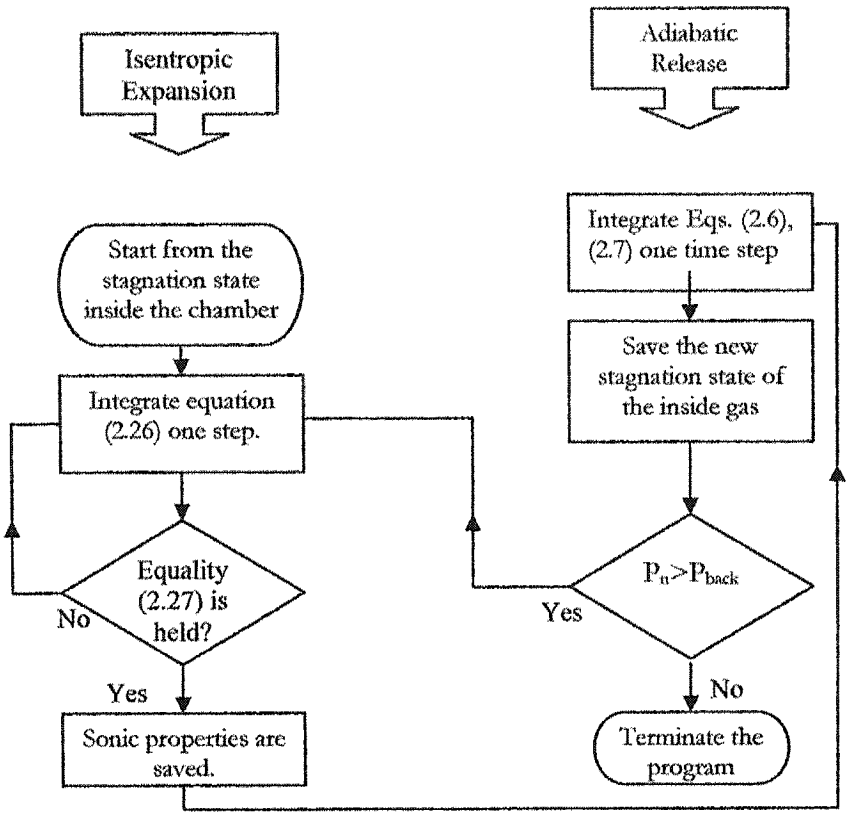

***Fig. 2.2**: Flowchart of the adiabatic gas release algorithm.*

2.5.2 Adiabatic Release

In an adiabatic gas release, the system of ordinary differential equations (2.6) and (2.7) are numerically solved. The initial condition is the initial stagnation state inside the chamber. Numerical integration stops when the pressure at the throat reaches to the ambient pressure P_{back}. Each integration step results in new values of specific volume and internal energy. The corresponding new value of temperature is obtained through an iterative solution of equation (2.24). Equations (2.6) and (2.7) are integrated using the first-order Euler method with a time step of 10^{-6} sec. The secant method is applied to solve equation (2.24) for temperature. The initial guesses are the temperature predicted by the ideal gas law and its perturbed value by 1%.

The analytical model developed in this chapter is applied to calculate time histories of thermodynamic properties of hydrogen inside the chamber and at the orifice; e.g., time-decays of stagnation and sonic pressures, temperatures and densities. In order to verify the analytical model, we simulate the hydrogen release from a chamber for ideal gas condition and compare the results to the exact solution given by [17]:

$$t = \frac{-2\Psi\left[\left(\frac{P}{P_\circ}\right)^{(1-\gamma)/2\gamma} - 1\right]}{(1-\gamma)R\sqrt{T_\circ}A_n\sqrt{\frac{\gamma}{R}\left(\frac{2}{\gamma+1}\right)^{(\gamma+1)/(\gamma-1)}}}, \tag{2.28}$$

where $P_\circ$ and $T_\circ$ represent initial pressure and temperature of the gas inside the chamber and are equal to 34.5 MPa and 300 °K, respectively. The specific heats are assumed to be constant throughout the release. γ is equal to 1.409. The volume of the chamber and the surface area of the throat are denoted by Ψ and A_n, and are equal to 2.7253×10^{-2} m^3 and 3.17×10^{-5} m^2. To obtain the analytical simulation for ideal gas condition, we set all coefficients of Beattie-Bridgeman EOS ($A_\circ$, $B_\circ$, α, b, and c) equal to zero. The time-decay of the stagnation pressure inside the chamber is shown in fig. 2.3, where the simulation of the analytical model for ideal gas condition and the exact solution given by equation (2.28) are compared to each other. A maximum relative error of 0.5% exists between the exact solution and the analytical model. The relative error increases with time and the maximum corresponds to the final simulation time.

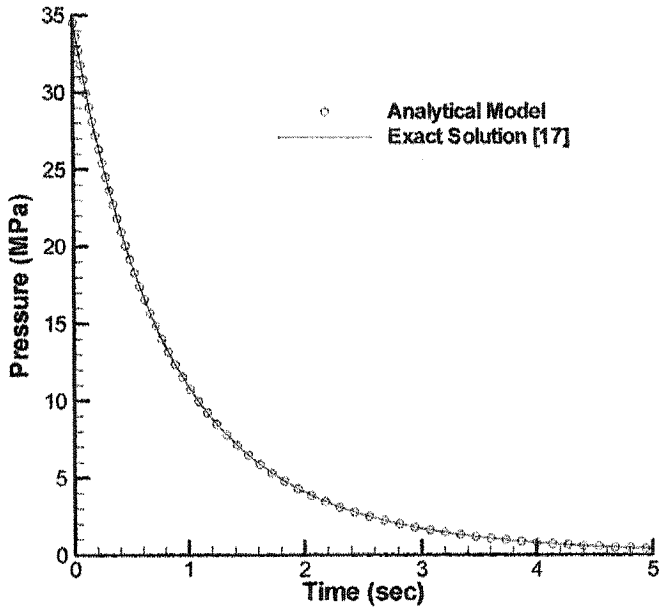

Fig. 2.3: *Time histories of stagnation pressures inside the chamber calculated from the analytical model and the exact solution for ideal gas condition; hydrogen is released from a reservoir at initial pressure and temperature of 34.5 and 300 °K.*

In Chapter 3, a finite volume code is modified to take into account the real gas effects at high pressures. Thermodynamic relations developed in Chapter 2 are applied in modifications.

Chapter 3

NUMERICAL SIMULATION

3.1 Problem Definition

An existing Euler solver, [21], is modified to simulate the discharge of hydrogen from a high-pressure chamber. The computational domain consists of a 60-degree wedge of an axisymmetric chamber. This particular geometry allows us to generate a fine and high-quality mesh at the throat and exit area without having a huge number of mesh nodes and elements that slow down the numerical computation. Hydrogen is released adiabatically to the atmospheric air. Viscosity is neglected and Euler equations are solved. The code is based on an implicit scheme, which has an accuracy of the first and second orders in time and space, respectively. Fluxes are calculated using Roe's averaging method, [22, 23]. To apply this code to simulate the real gas flows; transformation matrices, Jacobians, left and right eigenvectors and the definitions of Roe's averaged values are modified.

The computational domain is discretized into an unstructured tetrahedral mesh shown in fig. 3.1. The mesh is generated by GAMBIT 2.0.4. [30].

In this chapter, the original solver is described at first. Then, transformation matrices, Jacobians, eigenvectors, and Roe's averaged values are derived both for the real and ideal gas conditions. The treatment of the boundary conditions is discussed at the end of the chapter.

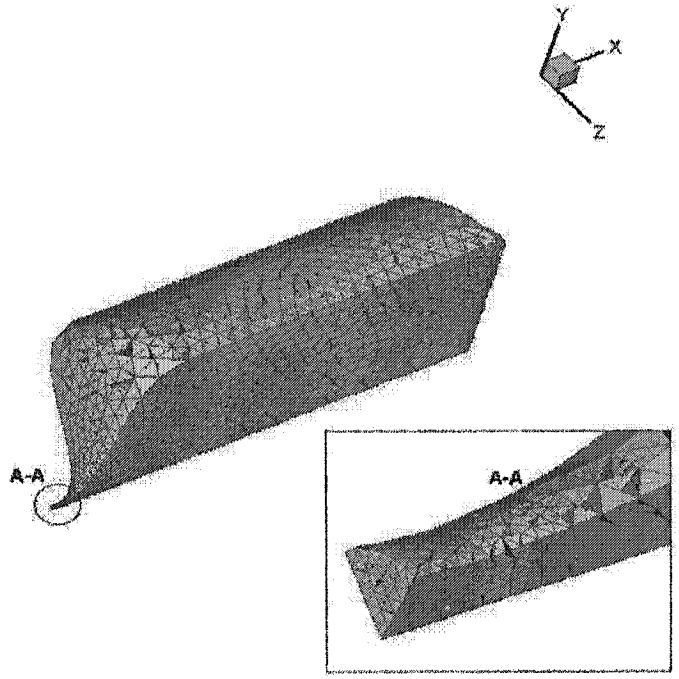

Fig. 3.1: *The 60-degree Wedge of the cylindrical chamber with unstructured tetrahedral mesh.*

3.2 Implicit Euler Scheme

When the viscosity and heat conductivity effects are negligible, the flow can be modeled by the Euler equations that represent the conservations of mass, momentum and energy. The vector form of the system of Euler equations in the absence of any momentum and energy sources can be written as:

$$\frac{\partial \vec{U}}{\partial t} + \vec{\nabla}.\vec{\vec{F}}(U) = 0, \tag{3.1}$$

where $\vec{U}$ is the vector of conservative variables in the contrast to $\vec{Q}$ that represents the primitive variables. The components of $\vec{\vec{F}}$ are the convective fluxes. All are given by:

$$\vec{U}=\begin{bmatrix}\rho\\ \rho u\\ \rho v\\ \rho w\\ \rho E\end{bmatrix},\vec{Q}=\begin{bmatrix}\rho\\ u\\ v\\ w\\ P\end{bmatrix},\vec{\vec{F}}=\left(\vec{k}=\begin{bmatrix}\rho u\\ \rho u^2+P\\ \rho uv\\ \rho uw\\ \rho uH\end{bmatrix},\ \vec{g}=\begin{bmatrix}\rho v\\ \rho vu\\ \rho v^2+P\\ \rho vw\\ \rho vH\end{bmatrix},\ \vec{h}=\begin{bmatrix}\rho w\\ \rho wu\\ \rho wv\\ \rho w^2+P\\ \rho wH\end{bmatrix}\right). \tag{3.2}$$

E and H are total internal energy and total enthalpy, respectively, and can be written as:

$$E=i+\frac{1}{2}(u^2+v^2+w^2);\ \ H=E+\frac{P}{\rho}. \tag{3.3}$$

Equation (3.1) is discretized using an implicit finite volume procedure,

$$\left\|\tau_j^c\right\|\frac{\vec{U}_j^{n+1}-\vec{U}_j^{n}}{\Delta t}+\sum_{over\,\delta\tau_j^c}\vec{\vec{F}}_{\delta\tau_j^c}^{n+1}\cdot\vec{n}_{\delta\tau_j^c}\Delta S_{\delta\tau_j^c}=0, \tag{3.4}$$

where j goes from 1 to the number of control volumes (nodes) that exist in the domain of computation. In our problem the mesh is fixed and the unit normal vectors $\vec{n}_{\delta\tau_j^c}$ and the surface area of the boundary faces $\Delta S_{\delta\tau_j^c}$ do not change with time.

Convective fluxes are nonlinear functions of conservative variables. The nonlinearity makes the solution of equations given by (3.4) a cumbersome process. The implicit convective fluxes are approximated by a linear Taylor expansion to avoid the solution of a nonlinear system of equations. The expansion gives:

$$\vec{\vec{F}}^{n+1}\cong\vec{\vec{F}}^{n}+\frac{\partial\vec{\vec{F}}}{\partial\vec{U}}^{n}\left(\vec{U}^{n+1}-\vec{U}^{n}\right). \tag{3.5}$$

$\frac{\partial\vec{\vec{F}}}{\partial\vec{U}}$ is called the conservative flux-Jacobian and its structure depends on the EOS describing the behavior of the gas. Substituting equation (3.5) in equation (3.4), we have:

$$\left\{\frac{\left\|\tau_j^c\right\|}{\Delta t}\vec{\vec{I}}+\sum_{over\,\delta\tau_j^c}\left(\frac{\partial\vec{\vec{F}}}{\partial\vec{U}}\right)_{\delta\tau_j^c}^{n}\cdot\vec{n}_{\delta\tau_j^c}\Delta S_{\delta\tau_j^c}\right\}\delta\vec{U}_j^{n+1}=-\sum_{over\,\delta\tau_j^c}\vec{\vec{F}}_{\delta\tau_j^c}^{n}\cdot\vec{n}_{\delta\tau_j^c}\Delta S_{\delta\tau_j^c}. \tag{3.6}$$

Several schemes can be employed to evaluate the convective fluxes at the boundary surfaces of the control volume, $\vec{\bar{F}}^{n}_{\delta v_j^c}$. Roe's averaging method applied herein is among the most efficient schemes. The definition of Roe's averaged values is dependent on the EOS. We follow the method introduced by Glaister [8] to generalize Roe's average definitions. His work is based on a general EOS given by,

$$P = \varphi(\rho, i), \tag{3.7}$$

where density and internal energy are considered as independent variables. In the Beattie-Bridgeman EOS, which is already introduced as the reference EOS in this thesis, density and temperature are considered as independent variables. All the transformation matrices, Jacobians, eigenvectors, and Roe's averaged values that are developed later on in this chapter are based on the general EOS given by (3.7). The pressure derivatives P_i and P_ρ that appear in these equations are subsequently evaluated in terms of the derivatives and integrals of the Beattie-Bridgeman EOS to keep the compatibility with the analytical model developed in Chapter 2.

An iterative algorithm, the GMRES method [26], is applied to solve equation (3.6) for $\delta\vec{U}_j^{n+1}$. No preconditioner is used in the calculations. The iteration stops when the residual is less than 10^{-6},

$$\Gamma\left[\left(\delta\vec{U}_j^{n+1}\right)^{\kappa}\right] = \left|\frac{\left(\delta\vec{U}_j^{n+1}\right)^{\kappa+1} - \left(\delta\vec{U}_j^{n+1}\right)^{\kappa}}{\left(\delta\vec{U}_j^{n+1}\right)^{\kappa+1}}\right| < 10^{-6}, \tag{3.6a}$$

where κ represents the number of iterations. After stopping the iterations, the values of the conservative variables at the new time step are calculated from,

$$\vec{U}_j^{n+1} = \vec{U}_j^{n} + \delta\vec{U}_j^{n+1}. \tag{3.6b}$$

At the new time step, the same procedure is repeated to iterate equation (3.6) and calculate conservative variables from (3.6b). This process continues until either a specified simulation time limit is reached or the residual $\Gamma\left[\vec{U}_j^{\kappa}\right]$ is less than 10^{-8}. The solution algorithm is explained with more details in [21]. The flowchart of this algorithm is shown in fig. 3.2.

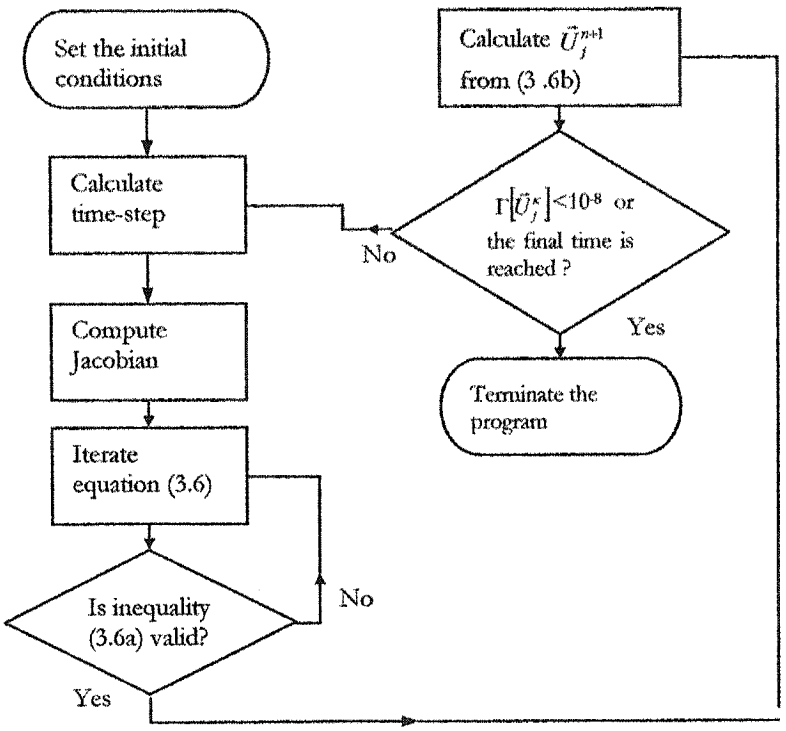

Fig. 3.2: *Flowchart of the solution algorithm of equations (3.6), and (3.6b).*

3.3 Transformation Matrices

3.3.1 Speed of Sound and Pressure Derivatives

Before starting the development of transformation matrices, we prove the following relation between the sound velocity and the pressure derivatives that is frequently referred to in upcoming sections:

$$a^2 = \frac{PP_i}{\rho^2} + P_\rho. \tag{3.8}$$

We begin from the definition of sound velocity and expand the isentropic pressure derivative according to equation (3.7),

$$a^2 = \left(\frac{\partial P}{\partial \rho}\right)_s = \left(\frac{\partial P}{\partial \rho}\right)_i \left(\frac{\partial \rho}{\partial \rho}\right)_s + \left(\frac{\partial P}{\partial i}\right)_\rho \left(\frac{\partial i}{\partial \rho}\right)_s = \left(\frac{\partial P}{\partial \rho}\right)_i + \left(\frac{\partial P}{\partial i}\right)_\rho \left(\frac{\partial i}{\partial \rho}\right)_s. \tag{3.9}$$

To obtain the isentropic derivative of the internal energy with respect to the density, we can write [18],

$$di = Tds - Pd\upsilon = Tds + \frac{P}{\rho^2} d\rho. \tag{3.10}$$

In an isentropic process,

$$di = \frac{p}{\rho^2} d\rho \Rightarrow \left(\frac{\partial i}{\partial \rho}\right)_s = \frac{P}{\rho^2}. \tag{3.11}$$

Substituting (3.11) in (3.9), we have:

$$\therefore a^2 = \left(\frac{\partial P}{\partial \rho}\right)_i + \left(\frac{\partial P}{\partial i}\right)_\rho \frac{P}{\rho^2} = P_\rho + \frac{PP_i}{\rho^2}. \tag{3.12}$$

3.3.2 Primitive-Conservative Transformations

The transformation matrices between the primitive and conservative variables, $[M]$ and $[M^{-1}]$, are defined so that,

$$[M] = \left[\frac{\partial \vec{U}}{\partial \vec{Q}}\right], \qquad [M^{-1}] = \left[\frac{\partial \vec{Q}}{\partial \vec{U}}\right], \qquad [M][M^{-1}] = 1. \tag{3.13}$$

$[M]$ can be calculated by direct differentiation as,

$$[M]=\begin{bmatrix} 1 & 0 & 0 & 0 & 0 \\ u & \rho & 0 & 0 & 0 \\ v & 0 & \rho & 0 & 0 \\ w & 0 & 0 & \rho & 0 \\ \rho\left(\frac{\partial i}{\partial \rho}\right)_P + i + \frac{V^2}{2} & \rho u & \rho v & \rho w & \rho\left(\frac{\partial i}{\partial p}\right)_\rho \end{bmatrix}. \tag{3.14}$$

Considering general EOS (3.7), we define the following pressure derivatives,

$$P_i = \left(\frac{\partial P}{\partial i}\right)_\rho = \left(\frac{\partial \varphi}{\partial i}\right)_\rho, \tag{3.15}$$

$$P_\rho = \left(\frac{\partial P}{\partial \rho}\right)_i = \left(\frac{\partial \varphi}{\partial \rho}\right)_i. \tag{3.16}$$

The derivative of the internal energy with respect to the density that appeared in (3.14) is rewritten as,

$$\left(\frac{\partial i}{\partial \rho}\right)_P = -\frac{\left(\frac{\partial P}{\partial \rho}\right)_i}{\left(\frac{\partial P}{\partial i}\right)_\rho} = -\frac{P_\rho}{P_i}. \tag{3.17}$$

According to the definition of the sound velocity in (3.12), we can write:

$$\rho\left(\frac{\partial i}{\partial \rho}\right)_P = -\frac{\rho}{P_i}\left(a^2 - \frac{PP_i}{\rho^2}\right) = -\frac{\rho a^2}{P_i} + \frac{P}{\rho}. \tag{3.18}$$

Substituting equations (3.15) and (3.18) in (3.14) and using the definition of the total enthalpy given by (3.3), we get the final form of the transformation matrix,

$$[M]=\left[\frac{\partial \vec{U}}{\partial \vec{Q}}\right]=\begin{bmatrix} 1 & 0 & 0 & 0 & 0 \\ u & \rho & 0 & 0 & 0 \\ v & 0 & \rho & 0 & 0 \\ w & 0 & 0 & \rho & 0 \\ H - \frac{\rho a^2}{P_i} & \rho u & \rho v & \rho w & \frac{\rho}{P_i} \end{bmatrix}. \tag{3.19}$$

Matrix $\left[M^{-1}\right]$ is obtained by following a similar procedure,

$$\left[M^{-1}\right]=\begin{bmatrix} 1 & 0 & 0 & 0 & 0 \\ \frac{-u}{\rho} & \frac{1}{\rho} & 0 & 0 & 0 \\ \frac{-v}{\rho} & 0 & \frac{1}{\rho} & 0 & 0 \\ \frac{-w}{\rho} & 0 & 0 & \frac{1}{\rho} & 0 \\ a^2+\frac{P_i}{\rho}\left(V^2-H\right) & \frac{-uP_i}{\rho} & \frac{-vP_i}{\rho} & \frac{-wP_i}{\rho} & \frac{P_i}{\rho} \end{bmatrix}. \tag{3.20}$$

3.3.3 Real Gas Application

Matrices (3.19) and (3.20) are given based on the general EOS (3.7). To apply them to the numerical simulation of hydrogen release in our problem, pressure derivatives P_i and P_ρ should be evaluated in terms of the derivatives or integrals of the Beattie-Bridgeman EOS (2.1). Considering density (specific volume) and temperature as the independent variables, we write the following expansion for P_i,

$$P_i=\left(\frac{\partial P}{\partial i}\right)_\rho=\left(\frac{\partial P}{\partial \rho}\right)_T\left(\frac{\partial \rho}{\partial i}\right)_\rho+\left(\frac{\partial P}{\partial T}\right)_\rho\left(\frac{\partial T}{\partial i}\right)_\rho=\left(\frac{\partial P}{\partial T}\right)_\rho\left(\frac{\partial T}{\partial i}\right)_\rho. \tag{3.21}$$

Using the notations introduced in Chapter 2,

$$P_i=\frac{f_T}{i_T}. \tag{3.22}$$

where i_T is obtained by differentiating equation (2.24) with respect to temperature at constant density or specific volume. The analytical expression for i_T is given in table 2.2.

Expanding similarly for the pressure derivative P_ρ, we get:

$$P_\rho=\left(\frac{\partial P}{\partial \rho}\right)_i=\left(\frac{\partial P}{\partial \rho}\right)_T\left(\frac{\partial \rho}{\partial \rho}\right)_i+\left(\frac{\partial P}{\partial T}\right)_\rho\left(\frac{\partial T}{\partial \rho}\right)_i=\left(\frac{\partial P}{\partial \rho}\right)_T+\left(\frac{\partial P}{\partial T}\right)_\rho\left(\frac{\partial T}{\partial \rho}\right)_i. \tag{3.23}$$

The partial derivatives on the right hand side of equation (3.23) are recast into the following forms so that they can be evaluated in terms of the expressions developed in Chapter 2:

$$\left(\frac{\partial P}{\partial \rho}\right)_T = -\upsilon^2\left(\frac{\partial P}{\partial \upsilon}\right)_T, \tag{3.24}$$

$$\left(\frac{\partial T}{\partial \rho}\right)_i = -\upsilon^2\left(\frac{\partial T}{\partial \upsilon}\right)_i = \upsilon^2 \frac{\left(\frac{\partial i}{\partial \upsilon}\right)_T}{\left(\frac{\partial i}{\partial T}\right)_\upsilon}. \tag{3.25}$$

After substituting equations (3.25) and (3.24) into equation (3.23), the pressure derivative is written as,

$$P_\rho = \upsilon^2\left(\frac{f_T i_\upsilon}{i_T} - f_\upsilon\right), \tag{3.26}$$

where i_υ is given in table 2.2 and represents the derivative of equation (2.24) with respect to specific volume while temperature is kept constant.

P_i and P_ρ should be replaced with equations (3.22) and (3.26) in the matrices and vectors obtained in this chapter based on the general EOS (3.7).

3.3.4 Ideal Gas Application

To verify our derivations in this chapter, we evaluate matrices and vectors for ideal gas conditions and compare the results to the corresponding relations in [22].

The ideal gas EOS can be written as:

$$P = \rho(\gamma - 1)i, \tag{3.27}$$

from which,

$$P_i = \rho(\gamma - 1), \tag{3.28}$$

$$P_\rho = (\gamma - 1)i. \tag{3.29}$$

The conservative-primitive transformation matrices for ideal gas condition are calculated by substituting (3.28) and (3.29) for pressure derivatives in matrices (3.19) and (3.20),

$$[M] = \begin{bmatrix} 1 & 0 & 0 & 0 & 0 \\ u & \rho & 0 & 0 & 0 \\ v & 0 & \rho & 0 & 0 \\ w & 0 & 0 & \rho & 0 \\ \frac{V^2}{2} & \rho u & \rho v & \rho w & \frac{1}{\gamma - 1} \end{bmatrix}, \tag{3.30}$$

$$[M^{-1}] = \begin{bmatrix} 1 & 0 & 0 & 0 & 0 \\ \frac{-u}{\rho} & \frac{1}{\rho} & 0 & 0 & 0 \\ \frac{-v}{\rho} & 0 & \frac{1}{\rho} & 0 & 0 \\ \frac{-w}{\rho} & 0 & 0 & \frac{1}{\rho} & 0 \\ \frac{\gamma - 1}{2} V^2 & -u(\gamma - 1) & -v(\gamma - 1) & -w(\gamma - 1) & \gamma - 1 \end{bmatrix}. \tag{3.31}$$

Equations (3.30) and (3.31) are exactly the transformation matrices given in [22].

3.4 Flux Jacobian Matrices

3.4.1 Conservative Jacobian Matrices

According to the definition, conservative Jacobian matrices that appear in equation (3.5) are the derivatives of the conservative fluxes with respect to the conservative variables. The Jacobian matrices are obtained by direct differentiation of the flux vectors given by equations (3.2) with respect to the conservative variables $\vec{U}$. New independent variables ρ, m, o, l and ε are defined for differentiations,

$$\vec{U}=\begin{bmatrix}\rho\\ m\\ o\\ l\\ \varepsilon\end{bmatrix},\vec{\vec{F}}=\left(\vec{k}=\begin{bmatrix}m\\ \frac{m^2}{\rho}+P\\ \frac{mo}{\rho}\\ \frac{ml}{\rho}\\ m\left(\frac{\varepsilon}{\rho}+\frac{P}{\rho}\right)\end{bmatrix},\ \vec{g}=\begin{bmatrix}o\\ \frac{mo}{\rho}\\ \frac{o^2}{\rho}+P\\ \frac{ol}{\rho}\\ o\left(\frac{\varepsilon}{\rho}+\frac{P}{\rho}\right)\end{bmatrix},\ \vec{h}=\begin{bmatrix}l\\ \frac{ml}{\rho}\\ \frac{ol}{\rho}\\ \frac{l^2}{\rho}+P\\ l\left(\frac{\varepsilon}{\rho}+\frac{P}{\rho}\right)\end{bmatrix}\right). \tag{3.32}$$

From equation (3.3),

$$i=\frac{\varepsilon}{\rho}-\frac{1}{2\rho^2}\left(m^2+o^2+l^2\right). \tag{3.33}$$

Equation (3.7) can be written as,

$$P=\varphi(\rho,i)=\varphi\left(\rho,i(\rho,m,o,l,\varepsilon)\right). \tag{3.34}$$

The pressure derivatives are calculated from (3.33) and (3.34) by the use of the chain rule of differentiations,

$$\frac{\partial P}{\partial m}=\left(\frac{\partial P}{\partial \rho}\right)_i\left(\frac{\partial \rho}{\partial m}\right)+\left(\frac{\partial P}{\partial i}\right)_\rho\left(\frac{\partial i}{\partial m}\right)=P_i\left(\frac{\partial i}{\partial m}\right)=-\frac{m}{\rho^2}P_i, \tag{3.35}$$

$$\frac{\partial P}{\partial o}=\left(\frac{\partial P}{\partial \rho}\right)_i\left(\frac{\partial \rho}{\partial o}\right)+\left(\frac{\partial P}{\partial i}\right)_\rho\left(\frac{\partial i}{\partial o}\right)=P_i\left(\frac{\partial i}{\partial o}\right)=-\frac{o}{\rho^2}P_i, \tag{3.36}$$

$$\frac{\partial P}{\partial l}=\left(\frac{\partial P}{\partial \rho}\right)_i\left(\frac{\partial \rho}{\partial l}\right)+\left(\frac{\partial P}{\partial i}\right)_\rho\left(\frac{\partial i}{\partial l}\right)=P_i\left(\frac{\partial i}{\partial l}\right)=-\frac{l}{\rho^2}P_i, \tag{3.37}$$

$$\frac{\partial P}{\partial \rho}=\left(\frac{\partial P}{\partial \rho}\right)_i\left(\frac{\partial \rho}{\partial \rho}\right)+\left(\frac{\partial P}{\partial i}\right)_\rho\left(\frac{\partial i}{\partial \rho}\right)=P_\rho+\left(-\frac{\varepsilon}{\rho^2}+\frac{m^2+o^2+l^2}{\rho^3}\right)P_i, \tag{3.38}$$

$$\frac{\partial P}{\partial \varepsilon}=\left(\frac{\partial P}{\partial \rho}\right)_i\left(\frac{\partial \rho}{\partial \varepsilon}\right)+\left(\frac{\partial P}{\partial i}\right)_\rho\left(\frac{\partial i}{\partial \varepsilon}\right)=P_i\left(\frac{\partial i}{\partial \varepsilon}\right)=\frac{P_i}{\rho}. \tag{3.39}$$

Applying equations (3.35) to (3.39), we differentiate the components of the conservative flux $\vec{\vec{F}}$ to obtain the Jacobian matrices in all directions,

$$[A]=\left[\frac{\partial \vec{k}}{\partial \vec{U}}\right]= \tag{3.40}$$

$$\begin{bmatrix} 0 & 1 & 0 & 0 & 0 \\ -\frac{m^2}{\rho^2}+P_\rho & \frac{2m}{\rho}-\frac{m}{\rho^2}P_l & -\frac{o}{\rho^2}P_l & -\frac{l}{\rho^2}P_l & \frac{P_l}{\rho} \\ +P_l\left(\frac{m^2+o^2+l^2}{\rho^3}-\frac{\varepsilon}{\rho^2}\right) & & & & \\ -\frac{mo}{\rho^2} & \frac{o}{\rho} & \frac{m}{\rho} & 0 & 0 \\ -\frac{ml}{\rho^2} & \frac{l}{\rho} & 0 & \frac{m}{\rho} & 0 \\ -m\left\{\frac{\varepsilon}{\rho^2}+\frac{P}{\rho^2}\right. & & & & \\ \left.-\frac{1}{\rho}\left[P_\rho+P_l\left(\frac{m^2+o^2+l^2}{\rho^3}-\frac{\varepsilon}{\rho^2}\right)\right]\right\} & \left(\frac{\varepsilon}{\rho}+\frac{P}{\rho}\right)-\frac{m^2}{\rho^3}P_l & -\frac{mo}{\rho^3}P_l & -\frac{ml}{\rho^3}P_l & m\left(\frac{1}{\rho}+\frac{P_l}{\rho^2}\right) \end{bmatrix},$$

which can be reduced to,

$$[A]=\begin{bmatrix} 0 & 1 & 0 & 0 & 0 \\ a^2-u^2-\frac{P_l}{\rho}\left(H-V^2\right) & 2u-\frac{uP_l}{\rho} & -\frac{vP_l}{\rho} & -\frac{wP_l}{\rho} & \frac{P_l}{\rho} \\ -uv & v & u & 0 & 0 \\ -uw & w & 0 & u & 0 \\ u\left(a^2-H\right)-\frac{uP_l}{\rho}\left(H-V^2\right) & H-\frac{u^2P_l}{\rho} & -\frac{uvP_l}{\rho} & -\frac{uwP_l}{\rho} & u+\frac{uP_l}{\rho} \end{bmatrix}; \tag{3.41}$$

The Jacobian matrix in the y-direction is:

$$[B]=\left[\frac{\partial \vec{g}}{\partial \vec{U}}\right]= \tag{3.42}$$

$$\begin{bmatrix} 0 & 0 & 1 & 0 & 0 \\ -\frac{mo}{\rho^2} & \frac{o}{\rho} & \frac{m}{\rho} & 0 & 0 \\ -\frac{o^2}{\rho^2}+P_\rho & -\frac{m}{\rho^2}P_l & \frac{2o}{\rho}-\frac{o}{\rho^2}P_l & -\frac{l}{\rho^2}P_l & \frac{P_l}{\rho} \\ +P_l\left(\frac{m^2+o^2+l^2}{\rho^3}-\frac{\varepsilon}{\rho^2}\right) & & & & \\ -\frac{ol}{\rho^2} & 0 & \frac{l}{\rho} & \frac{o}{\rho} & 0 \\ -o\left\{\frac{\varepsilon}{\rho^2}+\frac{P}{\rho^2}\right. & & & & \\ \left.-\frac{1}{\rho}\left[P_\rho+P_l\left(\frac{m^2+o^2+l^2}{\rho^3}-\frac{\varepsilon}{\rho^2}\right)\right]\right\} & -\frac{mo}{\rho^3}P_l & \left(\frac{\varepsilon}{\rho}+\frac{P}{\rho}\right)-\frac{o^2}{\rho^3}P_l & -\frac{ol}{\rho^3}P_l & o\left(\frac{1}{\rho}+\frac{P_l}{\rho^2}\right) \end{bmatrix},$$

or,

$$[B]=\begin{bmatrix} 0 & 0 & 1 & 0 & 0 \\ -uv & v & u & 0 & 0 \\ a^2-v^2-\frac{P_i}{\rho}\left(H-V^2\right) & -\frac{uP_i}{\rho} & 2v-\frac{vP_i}{\rho} & -\frac{wP_i}{\rho} & \frac{P_i}{\rho} \\ -vw & 0 & w & v & 0 \\ v\left(a^2-H\right)-\frac{vP_i}{\rho}\left(H-V^2\right) & -\frac{uvP_i}{\rho} & H-\frac{v^2P_i}{\rho} & -\frac{vwP_i}{\rho} & v+\frac{vP_i}{\rho} \end{bmatrix}; \tag{3.43}$$

The Jacobian matrix in the z-direction is given by:

$$[C]=\left[\frac{\partial\vec{h}}{\partial\vec{U}}\right]= \tag{3.44}$$

$$\begin{bmatrix} 0 & 0 & 0 & 1 & 0 \\ -\frac{ml}{\rho^2} & \frac{l}{\rho} & 0 & \frac{m}{\rho} & 0 \\ -\frac{ol}{\rho^2} & 0 & \frac{l}{\rho} & \frac{o}{\rho} & 0 \\ -\frac{l^2}{\rho^2}+P_\rho & -\frac{m}{\rho^2}P_i & -\frac{o}{\rho^2}P_i & \frac{2l}{\rho}-\frac{l}{\rho^2}P_i & \frac{P_i}{\rho} \\ +P_i\left(\frac{m^2+o^2+l^2}{\rho^3}-\frac{\varepsilon}{\rho^2}\right) & & & & \\ -l\left\{\frac{\varepsilon}{\rho^2}+\frac{P}{\rho^2}\right. & -\frac{ml}{\rho^3}P_i & -\frac{ol}{\rho^3}P_i & \left(\frac{\varepsilon}{\rho}+\frac{P}{\rho}\right)-\frac{l^2}{\rho^3}P_i & l\left(\frac{1}{\rho}+\frac{P_i}{\rho^2}\right) \\ \left.-\frac{1}{\rho}\left[P_\rho+P_i\left(\frac{m^2+o^2+l^2}{\rho^3}-\frac{\varepsilon}{\rho^2}\right)\right]\right\} & & & & \end{bmatrix},$$

that is reduced to,

$$[C]=\begin{bmatrix} 0 & 0 & 0 & 1 & 0 \\ -uw & w & 0 & u & 0 \\ -vw & 0 & w & v & 0 \\ a^2-w^2-\frac{P_i}{\rho}\left(H-V^2\right) & -\frac{uP_i}{\rho} & -\frac{vP_i}{\rho} & 2w-\frac{wP_i}{\rho} & \frac{P_i}{\rho} \\ w\left(a^2-H\right)-\frac{wP_i}{\rho}\left(H-V^2\right) & -\frac{uwP_i}{\rho} & -\frac{vwP_i}{\rho} & H-\frac{w^2P_i}{\rho} & w+\frac{wP_i}{\rho} \end{bmatrix}. \tag{3.45}$$

The Jacobian matrix in an arbitrary direction of $\vec{n}:\left(n_x,n_y,n_z\right)$ is calculated from equations (3.41), (3.43) and (3.45),

$$[K]=\frac{\partial\vec{\vec{F}}}{\partial\vec{U}}\cdot\vec{n}= \tag{3.46}$$

$$\begin{bmatrix}
0 & n_x & n_y & n_z & 0 \\
\left[a^2-\frac{P_I}{\rho}\left(H-V^2\right)\right]n_x-\vec{V}\cdot\vec{n} & \left(u-\frac{uP_I}{\rho}\right)n_x+\vec{V}\cdot\vec{n} & -\frac{vP_I}{\rho}n_x+un_y & -\frac{wP_I}{\rho}n_x+un_z & \frac{P_I}{\rho}n_x \\
\left[a^2-\frac{P_I}{\rho}\left(H-V^2\right)\right]n_y-\vec{V}\cdot\vec{n} & -\frac{uP_I}{\rho}n_y+vn_x & \left(v-\frac{vP_I}{\rho}\right)n_y+\vec{V}\cdot\vec{n} & -\frac{wP_I}{\rho}n_y+vn_z & \frac{P_I}{\rho}n_y \\
\left[a^2-\frac{P_I}{\rho}\left(H-V^2\right)\right]n_z-\vec{V}\cdot\vec{n} & -\frac{uP_I}{\rho}n_z+wn_x & -\frac{vP_I}{\rho}n_z+wn_y & \left(w-\frac{wP_I}{\rho}\right)n_z+\vec{V}\cdot\vec{n} & \frac{P_I}{\rho}n_z \\
\left[\left(a^2-H\right)-\frac{P_I}{\rho}\left(H-V^2\right)\right]\vec{V}\cdot\vec{n} & Hn_x-\frac{uP_I}{\rho}\left(\vec{V}\cdot\vec{n}\right) & Hn_y-\frac{vP_I}{\rho}\left(\vec{V}\cdot\vec{n}\right) & Hn_z-\frac{wP_I}{\rho}\left(\vec{V}\cdot\vec{n}\right) & \left(1+\frac{P_I}{\rho}\right)\vec{V}\cdot\vec{n}
\end{bmatrix},$$

where $\vec{V}\cdot\vec{n}$ is the inner product of the velocity vector $\vec{V}$ and the unit normal vector $\vec{n}$ given by,

$$\vec{V}\cdot\vec{n}=un_x+vn_y+wn_z. \tag{3.47}$$

To apply Jacobian matrices (3.41), (3.43), (3.45) or (3.46) to our problem in which the Beattie-Bridgeman EOS describes the behavior of the real gas, we have to replace pressure derivatives with equations (3.22) and (3.26). If equations (3.28) and (3.29) are substituted for the pressure derivatives, the Jacobians will be obtained for ideal gas condition, where the Jacobians are reduced to:

$$[A]=\begin{bmatrix}
0 & 1 & 0 & 0 & 0 \\
-u^2+\frac{\gamma-1}{2}V^2 & (3-\gamma)u & -(\gamma-1)v & -(\gamma-1)w & (\gamma-1) \\
-uv & v & u & 0 & 0 \\
-uw & w & 0 & u & 0 \\
-u\left[\gamma E-(\gamma-1)V^2\right] & \gamma E-\frac{\gamma-1}{2}(V^2+2u^2) & -(\gamma-1)uv & -(\gamma-1)uw & \gamma u
\end{bmatrix}, \tag{3.48}$$

$$[B]=\begin{bmatrix} 0 & 0 & 1 & 0 & 0 \\ -uv & v & u & 0 & 0 \\ -v^2+\frac{\gamma-1}{2}V^2 & -(\gamma-1)u & (3-\gamma)v & -(\gamma-1)w & (\gamma-1) \\ -vw & 0 & w & v & 0 \\ -v\left[\gamma E-(\gamma-1)V^2\right] & -(\gamma-1)uv & \gamma E-\frac{\gamma-1}{2}(V^2+2v^2) & -(\gamma-1)vw & \gamma v \end{bmatrix}, \tag{3.49}$$

$$[C]=\begin{bmatrix} 0 & 0 & 0 & 1 & 0 \\ -uw & w & 0 & u & 0 \\ -vw & 0 & w & v & 0 \\ -w^2+\frac{\gamma-1}{2}V^2 & -(\gamma-1)u & -(\gamma-1)vu & (3-\gamma)w & (\gamma-1) \\ -w\left[\gamma E-(\gamma-1)V^2\right] & -(\gamma-1)uw & -(\gamma-1)vw & \gamma E-\frac{\gamma-1}{2}(V^2+2w^2) & \gamma w \end{bmatrix}. \tag{3.50}$$

Matrices (3.48) to (3.50) are exactly the conservative Jacobian matrices introduced in [22].

3.4.2 Primitive Jacobian Matrices

The primitive Jacobian matrices given by $[\widetilde{A}]$, $[\widetilde{B}]$ and $[\widetilde{C}]$ are defined as the derivatives of the primitive fluxes with respect to the primitive variables. They can be directly determined from the conservation equations written in terms of the primitive variables,

$$\frac{\partial \vec{Q}}{\partial t}+[\widetilde{A}]\frac{\partial \vec{Q}}{\partial x}+[\widetilde{B}]\frac{\partial \vec{Q}}{\partial y}+[\widetilde{C}]\frac{\partial \vec{Q}}{\partial z}=0. \tag{3.51}$$

The conservation equations in the absence of any internal sources are written as,

$$\frac{\partial \rho}{\partial t}+\left(\vec{V}\cdot\vec{\nabla}\rho\right)+\rho\vec{\nabla}\cdot\vec{V}=0, \tag{3.52a}$$

$$\frac{\partial \vec{V}}{\partial t}+\left(\vec{V}\cdot\vec{\nabla}\right)\vec{V}+\frac{\vec{\nabla}P}{\rho}=0, \tag{3.52b}$$

$$\frac{\partial E}{\partial t}+\left(\vec{V}\cdot\vec{\nabla}\right)E+\frac{1}{\rho}\vec{\nabla}\cdot\left(\vec{V}P\right)=0. \tag{3.52c}$$

The system of equations (3.52) cannot be rearranged into the format given by (3.51) unless the last equation (3.52c) is transformed to an equation for pressure. Following the procedure described in [22] and Appendix B, we rewrite the energy equation as,

$$\frac{\partial P}{\partial t}+\left(\vec{V}\cdot\vec{\nabla}\right)P+\rho a^2\left(\vec{\nabla}\cdot\vec{V}\right)=0. \tag{3.52d}$$

Comparing the system of equations (3.52) with the equivalent vector form (3.51), we obtain the primitive Jacobians in the x, y and z-directions as:

$$[\widetilde{A}]=\begin{bmatrix} u & \rho & 0 & 0 & 0 \\ 0 & u & 0 & 0 & 1/\rho \\ 0 & 0 & u & 0 & 0 \\ 0 & 0 & 0 & u & 0 \\ 0 & \rho a^2 & 0 & 0 & u \end{bmatrix}, \tag{3.53}$$

$$[\widetilde{B}]=\begin{bmatrix} v & 0 & \rho & 0 & 0 \\ 0 & v & 0 & 0 & 0 \\ 0 & 0 & v & 0 & 1/\rho \\ 0 & 0 & 0 & v & 0 \\ 0 & 0 & \rho a^2 & 0 & v \end{bmatrix}, \tag{3.54}$$

$$[\widetilde{C}]=\begin{bmatrix} w & 0 & 0 & \rho & 0 \\ 0 & w & 0 & 0 & 0 \\ 0 & 0 & w & 0 & 0 \\ 0 & 0 & 0 & w & 1/\rho \\ 0 & 0 & 0 & \rho a^2 & w \end{bmatrix}. \tag{3.55}$$

The primitive Jacobian matrix in the direction of the arbitrary unit vector $\vec{n}:(n_x,n_y,n_z)$ is calculated by combining equations (3.53) to (3.55),

$$[\widetilde{K}]=\begin{bmatrix} \vec{V}\cdot\vec{n} & \rho n_x & \rho n_y & \rho n_z & 0 \\ 0 & \vec{V}\cdot\vec{n} & 0 & 0 & n_x/\rho \\ 0 & 0 & \vec{V}\cdot\vec{n} & 0 & n_y/\rho \\ 0 & 0 & 0 & \vec{V}\cdot\vec{n} & n_z/\rho \\ 0 & \rho a^2 n_x & \rho a^2 n_y & \rho a^2 n_z & \vec{V}\cdot\vec{n} \end{bmatrix}. \tag{3.56}$$

The structures of the primitive Jacobians are simpler than the conservative ones. They are directly determined from the conservation equations and no assumption has been made

regarding the EOS. Therefore the same primitive Jacobian matrices are applied to the ideal and the real gas conditions. In the next section, we use this property to calculate the eigenvectors of the conservative Jacobians for real gas condition from the eigenvectors of the primitive Jacobians (3.56).

3.5 Eigenvalues and Eigenvectors

3.5.1 Eigenvalues

In order to apply an upwind method, positive and negative fluxes should be determined. This requires the knowledge of the eigenvalues and eigenvectors of the Jacobian matrices. Having a simpler structure than that of the matrix (3.46), the primitive Jacobian matrix (3.56) is applied to eigenvalue analysis. Then the relation between the primitive and the conservative Jacobian matrices is obtained, which in turn results in a relation between the primitive and conservative eigenvectors.

Equation (3.1) can be rewritten as:

$$\frac{\partial \vec{U}}{\partial t}+[A]\frac{\partial \vec{U}}{\partial x}+[B]\frac{\partial \vec{U}}{\partial y}+[C]\frac{\partial \vec{U}}{\partial z}=0. \tag{3.57}$$

From the definition of the transformation matrices, we have:

$$[M]\frac{\partial \vec{Q}}{\partial t}+[A][M]\frac{\partial \vec{Q}}{\partial x}+[B][M]\frac{\partial \vec{Q}}{\partial y}+[C][M]\frac{\partial \vec{Q}}{\partial z}=0. \tag{3.58}$$

Multiplying both sides of equation (3.58) by $[M^{-1}]$,

$$\frac{\partial \vec{Q}}{\partial t}+[M^{-1}][A][M]\frac{\partial \vec{Q}}{\partial x}+[M^{-1}][B][M]\frac{\partial \vec{Q}}{\partial y}+[M^{-1}][C][M]\frac{\partial \vec{Q}}{\partial z}=0. \tag{3.59}$$

Comparing equation (3.59) with equation (3.51), we can easily figure out the following relations between the primitive and conservative Jacobian matrices:

$$
\begin{aligned}
[\tilde{A}] &= [M^{-1}][A][M], \\
[\tilde{B}] &= [M^{-1}][B][M], \\
[\tilde{C}] &= [M^{-1}][C][M], \\
[\tilde{K}] &= [M^{-1}][K][M].
\end{aligned}
\tag{3.60}
$$

Equations (3.60) imply that the conservative and primitive Jacobians $[K]$ and $[\tilde{K}]$ are connected together by a similarity transformation. It has been proved in linear algebra that the similarity-transformed matrices have the same eigenvalues [25]. The eigenvalues of the primitive Jacobian matrix $[\tilde{K}]$ are given in [22] as:

$$
\begin{aligned}
\lambda_1 &= \lambda_2 = \lambda_3 = un_x + vn_y + wn_z, \\
\lambda_4 &= un_x + vn_y + wn_z + a, \\
\lambda_5 &= un_x + vn_y + wn_z - a,
\end{aligned}
\tag{3.61}
$$

which can be equivalently called as the eigenvalues of the conservative Jacobian $[K]$ or the wave characteristics.

3.5.2 Eigenvectors

The left eigenvectors of matrix $[\tilde{K}]$ are denoted by $\vec{\tilde{l}}_j$, where j goes from 1 to 5. They are the solutions to the following system of equations,

$$
\vec{\tilde{l}}_j^{\,T}[\tilde{K}] = \lambda_j \vec{\tilde{l}}_j^{\,T}. \tag{3.62}
$$

The right eigenvectors of the Jacobian matrix $[\tilde{K}]$ are similarly defined and represented by $\vec{\tilde{r}}_j$ as:

$$
[\tilde{K}]\vec{\tilde{r}}_j = \lambda_j \vec{\tilde{r}}_j. \tag{3.63}
$$

Neither the left nor the right eigenvectors of the primitive Jacobian matrix are dependent on the EOS. They are given in [22] by,

$$\vec{\vec{l}}_1 = \begin{bmatrix} 1 \\ 0 \\ 0 \\ 0 \\ \frac{-1}{a^2} \end{bmatrix}, \vec{\vec{l}}_2 = \begin{bmatrix} 0 \\ -n_z \\ 0 \\ n_x \\ 0 \end{bmatrix}, \vec{\vec{l}}_3 = \begin{bmatrix} 0 \\ n_y \\ -n_x \\ 0 \\ 0 \end{bmatrix}, \vec{\vec{l}}_4 = \begin{bmatrix} 0 \\ n_x \\ n_y \\ n_z \\ \frac{1}{\rho a} \end{bmatrix}, \vec{\vec{l}}_4 = \begin{bmatrix} 0 \\ -n_x \\ -n_y \\ -n_z \\ \frac{1}{\rho a} \end{bmatrix}, \tag{3.64}$$

$$\vec{\vec{r}}_1 = \begin{bmatrix} 1 \\ 0 \\ 0 \\ 0 \\ 0 \end{bmatrix}, \vec{\vec{r}}_2 = \begin{bmatrix} 0 \\ -n_z \\ -\frac{n_y n_z}{n_x} \\ \frac{n_y^2 + n_x^2}{n_x} \\ 0 \end{bmatrix}, \vec{\vec{r}}_3 = \begin{bmatrix} 0 \\ n_y \\ -\frac{n_z^2 + n_x^2}{n_x} \\ \frac{n_y n_z}{n_x} \\ 0 \end{bmatrix}, \vec{\vec{r}}_4 = \begin{bmatrix} \frac{\rho}{2a} \\ \frac{n_x}{2} \\ \frac{n_y}{2} \\ \frac{n_z}{2} \\ \frac{\rho a}{2} \end{bmatrix}, \vec{\vec{r}}_5 = \begin{bmatrix} \frac{\rho}{2a} \\ -\frac{n_x}{2} \\ -\frac{n_y}{2} \\ -\frac{n_z}{2} \\ \frac{\rho a}{2} \end{bmatrix}. \tag{3.65}$$

Using equations (3.60), we can replace conservative Jacobians for primitive Jacobians in equations (3.62) and (3.63),

$$\begin{aligned} \vec{\vec{l}}_j^T [M^{-1}][K][M] &= \lambda_j \vec{\vec{l}}_j^T, \\ [M^{-1}][K][M]\vec{\vec{r}}_j &= \lambda_j \vec{\vec{r}}_j. \end{aligned} \tag{3.67}$$

or,

$$\begin{aligned} \vec{\vec{l}}_j^T [M^{-1}][K] &= \lambda_j \vec{\vec{l}}_j^T [M^{-1}], \\ [K][M]\vec{\vec{r}}_j &= \lambda_j [M]\vec{\vec{r}}_j. \end{aligned} \tag{3.68}$$

Equation (3.68) implies that the following relations exist between the conservative and primitive eigenvectors:

$$\vec{l}_j^T = \vec{\vec{l}}_j^T [M^{-1}], \tag{3.69}$$

$$\vec{r}_j = [M]\vec{\vec{r}}_j. \tag{3.70}$$

The left and right conservative eigenvectors are calculated through the matrix-vector multiplications of the primitive eigenvectors and the transformation matrices as described by (3.69) and (3.70).

The left eigenvector matrix $[L]$ is constructed so that its rows are the left eigenvectors of the conservative Jacobian given by (3.69). It is calculated as:

$$[L]=\begin{bmatrix} \frac{-P_i}{\rho a^2}\left(V^2-H\right) & \frac{uP_i}{\rho a^2} & \frac{vP_i}{\rho a^2} & \frac{wP_i}{\rho a^2} & \frac{-P_i}{\rho a^2} \\ \frac{un_z}{\rho}-\frac{wn_x}{\rho} & \frac{-n_z}{\rho} & 0 & \frac{n_x}{\rho} & 0 \\ \frac{-un_y}{\rho}+\frac{vn_x}{\rho} & \frac{n_y}{\rho} & \frac{-n_x}{\rho} & 0 & 0 \\ \frac{-un_x}{\rho}-\frac{vn_y}{\rho}-\frac{wn_x}{\rho} & \frac{n_x}{\rho}-\frac{uP_i}{\rho^2 a} & \frac{n_y}{\rho}-\frac{vP_i}{\rho^2 a} & \frac{n_z}{\rho}-\frac{wP_i}{\rho^2 a} & \frac{P_i}{\rho^2 a} \\ +\frac{a}{\rho}+\frac{P_i}{\rho^2 a}\left(V^2-H\right) & & & & \\ \frac{un_x}{\rho}+\frac{vn_y}{\rho}+\frac{wn_x}{\rho} & \frac{-n_x}{\rho}-\frac{uP_i}{\rho^2 a} & \frac{-n_y}{\rho}-\frac{vP_i}{\rho^2 a} & \frac{-n_z}{\rho}-\frac{wP_i}{\rho^2 a} & \frac{P_i}{\rho^2 a} \\ +\frac{a}{\rho}+\frac{P_i}{\rho^2 a}\left(V^2-H\right) & & & & \end{bmatrix} \tag{3.71}$$

The columns of the right eigenvector matrix consist of the right eigenvectors of the conservative Jacobian,

$$[R]= \tag{3.72}$$

$$\begin{bmatrix} 1 & 0 & 0 & \frac{\rho}{2a} & \frac{\rho}{2a} \\ u & -\rho n_z & \rho n_y & \frac{\rho u}{2a}+\frac{\rho n_x}{2} & \frac{\rho u}{2a}-\frac{\rho n_x}{2} \\ v & -\frac{\rho n_y n_z}{n_x} & -\frac{\rho\left(n_z^2+n_x^2\right)}{n_x} & \frac{\rho v}{2a}+\frac{\rho n_y}{2} & \frac{\rho v}{2a}-\frac{\rho n_y}{2} \\ w & \frac{\rho\left(n_y^2+n_x^2\right)}{n_x} & \frac{\rho n_y n_z}{n_x} & \frac{\rho w}{2a}+\frac{\rho n_z}{2} & \frac{\rho w}{2a}-\frac{\rho n_z}{2} \\ H-\frac{\rho a^2}{P_i} & -\rho u n_z-\frac{\rho v n_y n_z}{n_x} & \rho u n_y-\frac{\rho v\left(n_z^2+n_x^2\right)}{n_x} & \frac{\rho H}{2a}+\frac{\rho u n_x}{2}+ & \frac{\rho H}{2a}-\frac{\rho u n_x}{2}- \\ & +\frac{\rho w\left(n_y^2+n_x^2\right)}{n_x} & +\frac{\rho w n_y n_z}{n_x} & \frac{\rho v n_y}{2}+\frac{\rho w n_z}{2} & \frac{\rho v n_y}{2}-\frac{\rho w n_z}{2} \end{bmatrix}$$

In linear algebra [25], several properties have been proved for the left and the right eigenvector matrices; e.g., the matrix of the right eigenvectors $[R]$ is the inverse of the matrix of the left eigenvectors $[L]$ and vice versa; and the conservative Jacobian $[K]$ can be diagonalized by the use of $[R]$ and $[L]$ so that:

$$[L][K][R]=[\Lambda], \tag{3.73}$$

where $[\Lambda]$ is the diagonal matrix of eigenvalues (3.61).

The pressure derivatives P_i and P_ρ in matrices (3.71) and (3.72) should be replaced with equations (3.22) and (3.26) to find the right and left eigenvector matrices that are compatible with the Beattie-Bridgeman EOS, whereas in the ideal gas simulations, equations (3.28) and (3.29) give the required pressure derivatives. The left and the right eigenvector matrices for ideal gas condition are calculated as,

$$[L]= \tag{3.74}$$

$$\begin{bmatrix}
\frac{-(\gamma-1)}{a^2}\left(V^2-H\right) & \frac{u(\gamma-1)}{a^2} & \frac{v(\gamma-1)}{a^2} & \frac{w(\gamma-1)}{a^2} & \frac{(1-\gamma)}{a^2} \\
\frac{un_z}{\rho}-\frac{wn_x}{\rho} & \frac{-n_z}{\rho} & 0 & \frac{n_x}{\rho} & 0 \\
\frac{-un_y}{\rho}+\frac{vn_x}{\rho} & \frac{n_y}{\rho} & \frac{-n_x}{\rho} & 0 & 0 \\
\frac{-un_x}{\rho}-\frac{vn_y}{\rho}-\frac{wn_x}{\rho} & \frac{n_x}{\rho}-\frac{u(\gamma-1)}{\rho a} & \frac{n_y}{\rho}-\frac{v(\gamma-1)}{\rho a} & \frac{n_z}{\rho}-\frac{w(\gamma-1)}{\rho a} & \frac{(\gamma-1)}{\rho a} \\
+\frac{a}{\rho}+\frac{(\gamma-1)}{\rho a}\left(V^2-H\right) & & & & \\
\frac{un_x}{\rho}+\frac{vn_y}{\rho}+\frac{wn_x}{\rho} & \frac{-n_x}{\rho}-\frac{u(\gamma-1)}{\rho a} & \frac{-n_y}{\rho}-\frac{v(\gamma-1)}{\rho a} & \frac{-n_z}{\rho}-\frac{w(\gamma-1)}{\rho a} & \frac{(\gamma-1)}{\rho a} \\
+\frac{a}{\rho}+\frac{(\gamma-1)}{\rho a}\left(V^2-H\right) & & & &
\end{bmatrix},$$

$$[R] = \tag{3.75}$$

$$\begin{bmatrix} 1 & 0 & 0 & \frac{\rho}{2a} & \frac{\rho}{2a} \\ u & -\rho n_z & \rho n_y & \frac{\rho u}{2a}+\frac{\rho n_x}{2} & \frac{\rho u}{2a}-\frac{\rho n_x}{2} \\ v & -\frac{\rho n_y n_z}{n_x} & -\frac{\rho\left(n_z^2+n_x^2\right)}{n_x} & \frac{\rho v}{2a}+\frac{\rho n_y}{2} & \frac{\rho v}{2a}-\frac{\rho n_y}{2} \\ w & \frac{\rho\left(n_y^2+n_x^2\right)}{n_x} & \frac{\rho n_y n_z}{n_x} & \frac{\rho w}{2a}+\frac{\rho n_z}{2} & \frac{\rho w}{2a}-\frac{\rho n_z}{2} \\ H-\frac{a^2}{(\gamma-1)} & -\rho u n_z-\frac{\rho v n_y n_z}{n_x}+\frac{\rho w\left(n_y^2+n_x^2\right)}{n_x} & \rho u n_y-\frac{\rho v\left(n_z^2+n_x^2\right)}{n_x}+\frac{\rho w n_y n_z}{n_x} & \frac{\rho H}{2a}+\frac{\rho u n_x}{2}+\frac{\rho v n_y}{2}+\frac{\rho w n_z}{2} & \frac{\rho H}{2a}-\frac{\rho u n_x}{2}-\frac{\rho v n_y}{2}-\frac{\rho w n_z}{2} \end{bmatrix}.$$

3.6 Roe's Approximate Riemann Solver

As it is explained in Section 3.2, Roe's approximate Riemann solver is one of the most efficient methods to evaluate fluxes at the boundaries. In this section, we introduce the method for ideal gas condition. Then we explain the modifications introduced in [8] to apply the method to the real gas condition.

3.6.1 Definition of the problem

We consider two adjacent control volumes denoted by τ_j^c and τ_{j+1}^c in fig 3.3. The unit vector normal to the boundary surface between two control-volumes is given by $\vec{n}:\left(n_x,n_y,n_z\right)$. The conservative flux vector that goes from control volume j to control volume j+1 is given by:

$$\vec{F} = \vec{\vec{F}}_{\delta\tau} \cdot \vec{n} \tag{3.76}$$

The Roe's scheme can be stated as the following problem: Find the Jacobian matrix $[\hat{K}]=[\hat{K}(\vec{U}_j,\vec{U}_{j+1})]$ such that:

. $[\hat{K}(\vec{U}_j,\vec{U}_{j+1})]$ is diagonalizable and has independent eigenvectors;

. For any arbitrary $\vec{U}_j$ and $\vec{U}_{j+1}$, the following relation should be exactly satisfied:

$$\vec{F}_{j+1}-\vec{F}_j=[\hat{K}(\vec{U}_j,\vec{U}_{j+1})]\left(\vec{U}_{j+1}-\vec{U}_j\right) \tag{3.77}$$

. If $\vec{U}_j=\vec{U}_{j+1}=\vec{U}$ then $[\hat{K}(\vec{U}_j,\vec{U}_{j+1})]=[K]$.

Equation (3.77) can be considered as a first order approximation if the conservative Jacobian $[K]$ is substituted for the matrix $[\hat{K}]$, and $[K]$ is evaluated at node (j) or (j+1). But in Roe's scheme, we seek the averaged values that when the Jacobian $[K]$ is evaluated at, equation (3.77) becomes an exact equality. These averaged values are distinguished by a hat sign (∧). Once the averaged values are obtained, the conservative fluxes can be determined from the following relation [22]:

$$\vec{F}_{i\to j}^{Roe}=\frac{1}{2}(\vec{F}_j+\vec{F}_{j+1})-\frac{1}{2}[\hat{R}][|\Lambda|][\hat{L}]\left(\vec{U}_{j+1}-\vec{U}_j\right). \tag{3.78}$$

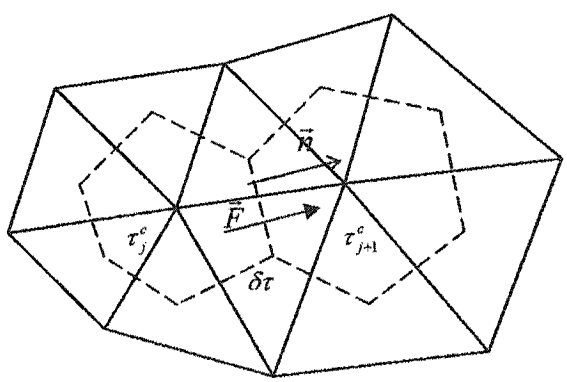

Fig. 3.3: *Schematic diagram of two adjacent control volumes and the flux vector crossing between them.*

3.6.2 Ideal Gas Application

The problem defined in the previous subsection has a unique solution when the thermodynamic properties of the flow are described by the ideal gas EOS. The solution is the set of the averaged variables given by [22]:

$$\begin{aligned}
&\hat{\rho} = \sqrt{\rho_j \rho_{j+1}}, \\
&\hat{u} = \frac{\sqrt{\rho_j}u_j + \sqrt{\rho_{j+1}}u_{j+1}}{\sqrt{\rho_j} + \sqrt{\rho_{j+1}}}, \qquad \hat{H} = \frac{\sqrt{\rho_j}H_j + \sqrt{\rho_{j+1}}H_{j+1}}{\sqrt{\rho_j} + \sqrt{\rho_{j+1}}}, \\
&\hat{v} = \frac{\sqrt{\rho_j}v_j + \sqrt{\rho_{j+1}}v_{j+1}}{\sqrt{\rho_j} + \sqrt{\rho_{j+1}}}, \qquad \hat{V}^2 = \hat{u}^2 + \hat{v}^2 + \hat{w}^2, \\
&\hat{w} = \frac{\sqrt{\rho_j}w_j + \sqrt{\rho_{j+1}}w_{j+1}}{\sqrt{\rho_j} + \sqrt{\rho_{j+1}}}, \qquad \hat{a}^2 = (\gamma - 1)\left(\hat{H} - \frac{\hat{V}^2}{2}\right).
\end{aligned} \tag{3.79}$$

Roe's fluxes are calculated from equation (3.78), where the left and the right eigenvector matrices, (3.74) and (3.75), as well as the diagonal eigenvalue matrix are evaluated at average values given in (3.79).

3.6.3 Real Gas Application

For real gas condition, the problem stated in Section 3.6.1 may have more than one solution or no solution at all. Several methods have been introduced in the literature [5-13]. The most classical approaches lead to the definition of the averaged pressure derivatives that satisfy the following equations,

$$\Delta P = \hat{P}_i \Delta i + \hat{P}_\rho \Delta \rho. \tag{3.80}$$

These averaged derivatives are not unique, and different definitions can be found at different works [5-12]. In this work we apply the definitions introduced by Glaister [8] that are based on the EOS (3.7):

$$\hat{P}_i = \begin{cases} \dfrac{1}{\Delta i}\left[\dfrac{P(\rho_{j+1},i_{j+1})+P(\rho_j,i_{j+1})}{2} - \dfrac{P(\rho_{j+1},i_j)+P(\rho_j,i_j)}{2}\right] & if\ \Delta i \neq 0 \\ \dfrac{P_i(\rho_{j+1},i)+P_i(\rho_j,i)}{2} & if\ \Delta i = 0 \end{cases} \tag{3.81}$$

and,

$$\hat{P}_\rho = \begin{cases} \dfrac{1}{\Delta \rho}\left[\dfrac{P(\rho_{j+1},i_{j+1})+P(\rho_{j+1},i_j)}{2} - \dfrac{P(\rho_j,i_{j+1})+P(\rho_j,i_j)}{2}\right] & if\ \Delta \rho \neq 0 \\ \dfrac{P_\rho(\rho,i_{j+1})+P_\rho(\rho,i_j)}{2} & if\ \Delta \rho = 0 \end{cases} \tag{3.82}$$

The following averaged variables are defined similarly for real gas condition:

$$\begin{aligned} &\hat{\rho} = \sqrt{\rho_j \rho_{j+1}}, \\ &\hat{u} = \frac{\sqrt{\rho_j}u_j + \sqrt{\rho_{j+1}}u_{j+1}}{\sqrt{\rho_j}+\sqrt{\rho_{j+1}}}, \quad \hat{H} = \frac{\sqrt{\rho_j}H_j + \sqrt{\rho_{j+1}}H_{j+1}}{\sqrt{\rho_j}+\sqrt{\rho_{j+1}}}, \\ &\hat{v} = \frac{\sqrt{\rho_j}v_j + \sqrt{\rho_{j+1}}v_{j+1}}{\sqrt{\rho_j}+\sqrt{\rho_{j+1}}}, \quad \hat{V}^2 = \hat{u}^2 + \hat{v}^2 + \hat{w}^2, \\ &\hat{w} = \frac{\sqrt{\rho_j}w_j + \sqrt{\rho_{j+1}}w_{j+1}}{\sqrt{\rho_j}+\sqrt{\rho_{j+1}}}, \quad \hat{p} = \hat{\rho}\left(\hat{H} - \hat{i} - \frac{\hat{V}^2}{2}\right), \\ &\hat{i} = \frac{\sqrt{\rho_j}i_j + \sqrt{\rho_{j+1}}i_{j+1}}{\sqrt{\rho_j}+\sqrt{\rho_{j+1}}}, \quad \hat{a}^2 = \hat{P}_\rho + \frac{\hat{P}\hat{P}_i}{\hat{\rho}^2}, \end{aligned} \tag{3.83}$$

where the averaged pressure is calculated in terms of the defined averaged enthalpy and internal energy. The averaged sound velocity is obtained from equation (3.8).

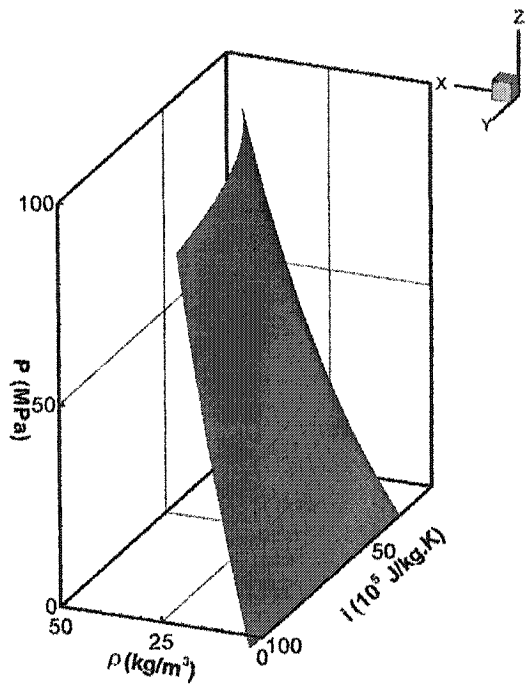

Fig. 3.4: *The convex surface of the pressure as a function of the density and the internal energy calculated from Beattie-Bridgeman EOS.*

The average values defined by equations (3.81) to (3.83) should be substituted in matrix $[K]$ given by equation (3.46) to calculate matrix $[\hat{K}]$. The resulting matrix is a solution to the problem stated in Section 3.6.1 if the real gas EOS given by equation (3.7) is convex, [27]. The convexity of the Beattie-Bridgeman EOS is shown in fig. 3.4.

3.7 Boundary Conditions

Two types of boundary conditions are implemented to simulate the hydrogen release from the 60-degree wedge shown in fig. 3.1: a free-slip boundary condition is applied to the walls and the cutting surfaces of the 60-degree wedge, and the exit surface is described by a supersonic outlet boundary condition.

3.7.1 Free-Slip Boundary Condition

The component of the velocity, which is normal to the boundary face ($\vec{V}\cdot\vec{n}$), is equal to zero when the boundary is described by the free-slip or non-penetrating condition. Both the solid walls and the cutting surfaces are treated using this type of boundary condition. When the normal velocity vanishes, the conservative flux vector crossing the boundary becomes,

$$\vec{F}=\vec{\vec{F}}_{\delta\tau}\cdot\vec{n}=\begin{bmatrix}0\\ Pn_x\\ Pn_y\\ Pn_z\\ 0\end{bmatrix}, \tag{3.84}$$

and the corresponding Jacobian is reduced to:

$$\begin{bmatrix}0 & 0 & 0 & 0 & 0\\ \left[a^2-\frac{P_i}{\rho}\left(H-V^2\right)\right]n_x & -\frac{uP_i}{\rho}n_x & -\frac{vP_i}{\rho}n_x & -\frac{wP_i}{\rho}n_x & \frac{P_i}{\rho}n_x\\ \left[a^2-\frac{P_i}{\rho}\left(H-V^2\right)\right]n_y & -\frac{uP_i}{\rho}n_y & -\frac{vP_i}{\rho}n_y & -\frac{wP_i}{\rho}n_y & \frac{P_i}{\rho}n_y\\ \left[a^2-\frac{P_i}{\rho}\left(H-V^2\right)\right]n_z & -\frac{uP_i}{\rho}n_z & -\frac{vP_i}{\rho}n_z & -\frac{wP_i}{\rho}n_z & \frac{P_i}{\rho}n_z\\ 0 & 0 & 0 & 0 & 0\end{bmatrix}. \tag{3.85}$$

The schematic diagram of a control volume located at the boundary surface is shown in fig. 3.5. No control volume or mesh node exists outside the boundary. Fluxes exiting the boundary surfaces cannot be calculated using the Roe's averaging method. The conservative fluxes and Jacobians at the free-slip boundary surfaces are evaluated at the corresponding boundary nodes (j).

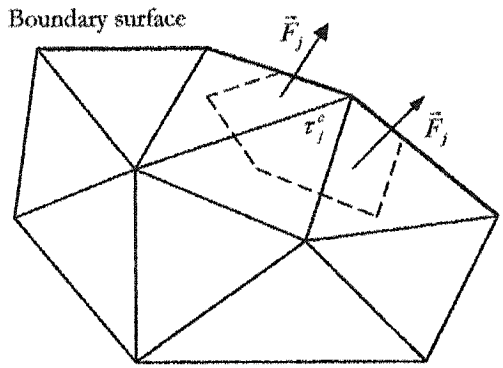

Fig. 3.5: *Schematic diagram of the control volume located at the boundary surface.*

3.7.2 Supersonic-Outlet Boundary Condition

According to the definition, all the wave characteristics given by equation (3.61) exit a supersonic-outlet boundary. This implies that no physical boundary condition is required for the definition of a supersonic outlet. One of the methods proposed in [22, 24] for the numerical treatment of this kind of boundaries is the extrapolation of conservative or primitive variables at the boundary based on the interior nodes. Having applied this method to simulate the hydrogen release in our problem, we were restricted to keep the CFL numbers ($a\Delta t/\Delta l$) less than 80 in order to avoid numerical instabilities. Using an Intel Pentium IV processor at 2.6GHz with 750MB memory, it took approximately five days to simulate 5 seconds of the hydrogen release at a CFL number of 80 for the mesh with 2452 mesh nodes. Another method was required to treat the supersonic outlet boundary condition.

As an alternative, the same method described in Section 3.7.1 is applied to the supersonic-outlet boundary; whereas, the corresponding fluxes and Jacobians are calculated from equations (3.2) and (3.46). Disregarding the Roe's averaging method, we evaluate

each flux-vector and Jacobian at the corresponding boundary node. The temporal increments of conservative variables at the outlet-boundary nodes, $\delta\vec{U}^{n+1}$, are determined together with the interior nodes from equation (3.6). No CFL number instability restriction is observed when this method is applied. The simulations are performed at CFL values up to 4000. The total CPU time to simulate 5 seconds of hydrogen release is reduced to 40 hours when CFL number is equal to 1000.

Fig 3.6 shows the velocity vector plot for real gas condition four seconds after the start of the release.

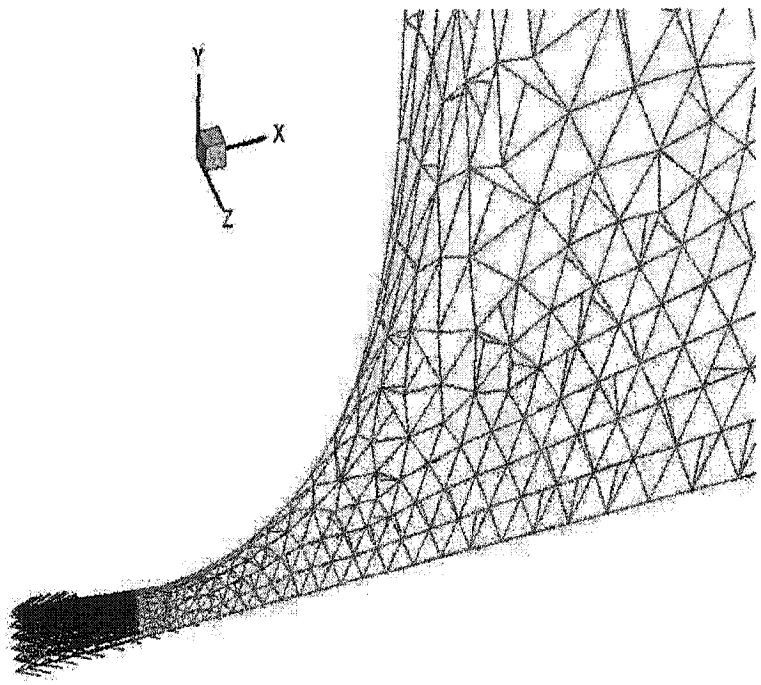

Fig. 3.6: *Velocity vector plot at t=4 sec.; hydrogen is releasing from a chamber, which was initially at a pressure and temperature of 34.5 MPa and 300 °K; real gas effects are considered.*

The following modifications have been done to the original finite volume code: the conservative Jacobians and eigenvector matrices are modified according to the Beattie-

Bridgman EOS. A generalized Roe's scheme is used to calculate the convective fluxes. Two types of boundary conditions are defined and applied to the code. These boundary conditions are exclusively defined and corrected to simulate the real gas release from a high-pressure chamber. Other boundary conditions may be required when the code is applied to simulate the real gas flow in different geometries. In the next chapter the simulation results for the hydrogen release are compared to the predictions obtained from the analytical model developed in Chapter 2.

Chapter 4

RESULTS

The results of the numerical simulations and predictions of the analytical model are compared to each other for hydrogen release from a high-pressure reservoir.

4.1 Problem Specifications

4.1.1 Geometrical Specifications

The finite-volume code is run to simulate the hydrogen release from a high-pressure cylinder. The flow accelerates through a converging part, a small diverging part and finally exits to the atmosphere. The diameter of the chamber is equal to 3.0×10^{-1} m. The entrance to the converging part has the same diameter as the chamber. The throat and the exit surface have areas of 3.17×10^{-5} m^2 and 3.73×10^{-5} m^2, respectively. The axial length of the diverging part is 3.45×10^{-3} m. The unstructured tetrahedral mesh is shown in fig. 3.1. There are 2452 mesh points that construct 9712 tetrahedral elements. The total volume of the elements is equal to 2.7253×10^{-2} m^3. The same throat surface area and total volume are applied to the analytical model to calculate the time histories of the stagnation and sonic properties of the gas inside the chamber and at the throat. The results obtained from the numerical simulation and the analytical model are compared together for ideal and real gas conditions.

4.1.2 Initial Conditions

The pressure and temperature of hydrogen are assumed to be initially uniform throughout the chamber. The initial pressure and temperature are equal to 34.5 MPa and 300° K, respectively. For the analytical model, the initial velocity of the flow is zero inside the chamber except at the throat where the flow is initialized at the sonic velocity that corresponds to the initial stagnation pressure and temperature of 34.5 MPa and 300° K. In the numerical simulation, hydrogen has a zero initial velocity throughout the chamber except for the exit surface that is initialized at an arbitrary supersonic velocity such as 1600 m/s. This arbitrary exit velocity is adjusted automatically after two or three time-iterations.

During the numerical and analytical simulations the pressure decreases with time everywhere inside the chamber as well as at the exit surface. The simulation stops when the flow pressure at the exit surface reaches the atmospheric back pressure.

4.1.3 Time Step Calculation Strategy

The analytical model developed in Chapter 2 involves two integration steps. The first one includes the time integration of the conservation equations (2.6) and (2.7), and the second one is the integration of the isentropic expansion equation (2.26) with respect to the specific volume for calculation of the sonic temperature of hydrogen at the throat. Since the predictions of the analytical model are used as a reference to validate the numerical simulation, integration errors should be kept as small as possible. The first order Euler method is applied to integrate foregoing equations. Using this low order method, we need to have very small integration steps, such as $\Delta t=10^{-6}$ sec. and $\Delta \upsilon=0.05\%\upsilon_t$, to obtain the required accuracy.

The local time step in the numerical simulation is determined for each mesh tetrahedron j from a predefined CFL number,

$$\Delta t_j = \frac{CFL}{a_j + |V_j|} \Delta l_j, \tag{4.1}$$

where a_j and $|V_j|$ are the speed of sound and the flow velocity at tetrahedron j, respectively. Δl_j represents the length scale corresponding to tetrahedron j. At each time iteration, overall time step is the minimum of the local time steps given by equation (4.1). Hydrogen has a small molecular weight (M=2.01588 gr.) and accelerates to velocities much higher than that of the air during an isentropic expansion; e.g., the ideal value of the speed of sound in hydrogen at a temperature of 300° K is about 1320 m/sec the corresponding value for air is equal to 340 m/sec. The high sound velocities result in small time-steps as calculated by equation (4.1). As a result, the unsteady simulation of the hydrogen release takes a huge amount of the CPU time as explained in Section 3.7.2; e.g., it takes around 40 hours to simulate 5 seconds of the hydrogen release at a CFL number of 1000.

The simulation starts with an initial CFL number of one and it is kept constant during the first 200 time-iterations. Then it is incremented with a constant rate of 10 units per time-iteration to a final given value. The results presented in the next section have been obtained using a final CFL number of 1000.

4.2 Simulation Results

The analytical and numerical simulation results are discussed in this section. The initial five seconds of the release are compared for ideal and real gas conditions. In this laps of time,

the total pressure drops from 34.5 MPa to less than 0.4 MPa, and 98.5% of the initial mass inside the chamber is released meanwhile the throat and the exit surface always remain at the sonic and supersonic conditions, respectively, for a back pressure of 0.1 MPa.

The velocity, pressure, temperature and density of the gas at the throat are depicted in figs (4.1) to (4.4). The numerical and analytical results for ideal and real gas conditions are compared together. For both the real and the ideal gas simulations, a maximum relative error of 2% exists between the analytical and the numerical simulations. The maximum relative error corresponds to the end of the release.

The initial values of the sound velocity predicted for real gas condition are higher than the corresponding values for ideal gas condition, fig. (4.1). Internal energy of a real gas includes not only the ideal part, which is related to the translational kinetic energies of molecules, but also contributions of vibrational and rotational energies. As the gas isentropically expands from stagnation state inside the chamber to the sonic state at the orifice, pressure decreases and hydrogen approaches ideal gas behavior. Some parts of energies that were already stored in the vibrational and rotational modes of internal energy are transformed into the kinetic energy of the flow. Therefore, at the start of the release, when the ideal and real gases expand from more and less the same stagnation states, the throat velocity for real gas condition is higher than the throat velocity for ideal gas condition. The sonic pressure decreases to lower values at the throat for real gas condition, fig. (4.2), because the real gas flow at the throat accelerates to higher velocities.

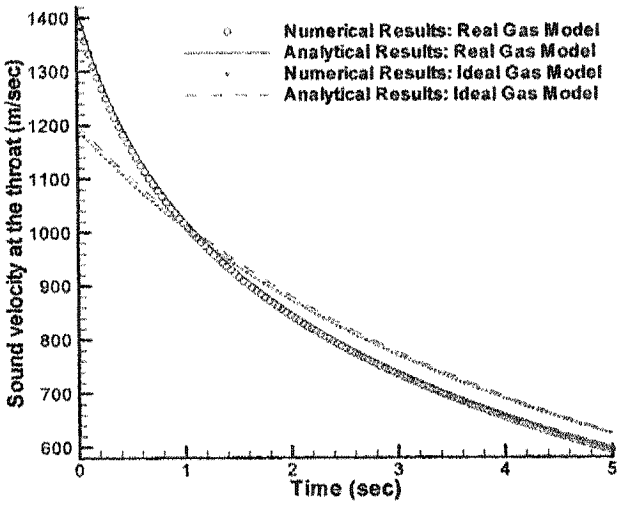

Fig. 4.1: *Analytical and numerical simulations of the flow velocity at the throat as a function of time for real and ideal gas conditions; hydrogen is released from a reservoir at initial pressure and temperature of 34.5 MPa and 300 °K.*

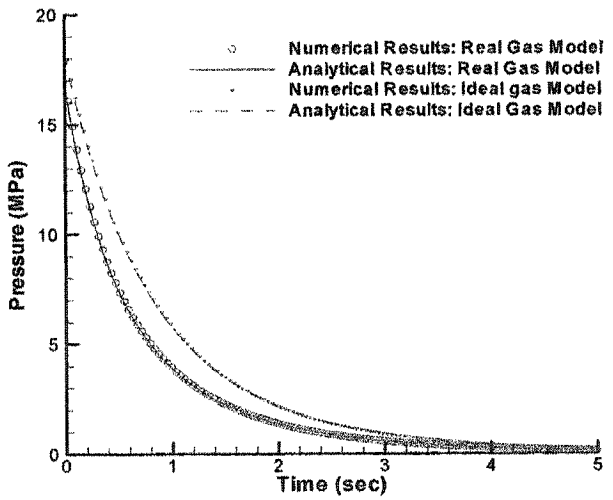

Fig. 4.2: *Analytical and numerical simulations of the flow pressure at the throat as a function of time for real and ideal gas conditions; hydrogen is released from a reservoir at initial pressure and temperature of 34.5 MPa and 300 °K.*

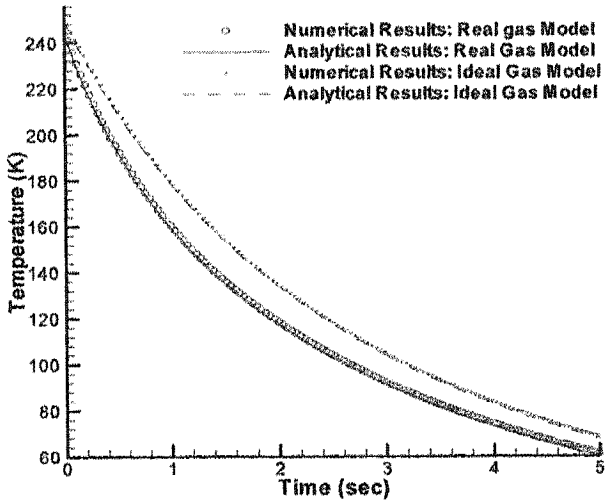

Fig. 4.3: *Analytical and numerical simulations of the flow temperature at the throat as a function of time for real and ideal gas conditions; hydrogen is released from a reservoir at initial pressure and temperature of 34.5 MPa and 300 °K.*

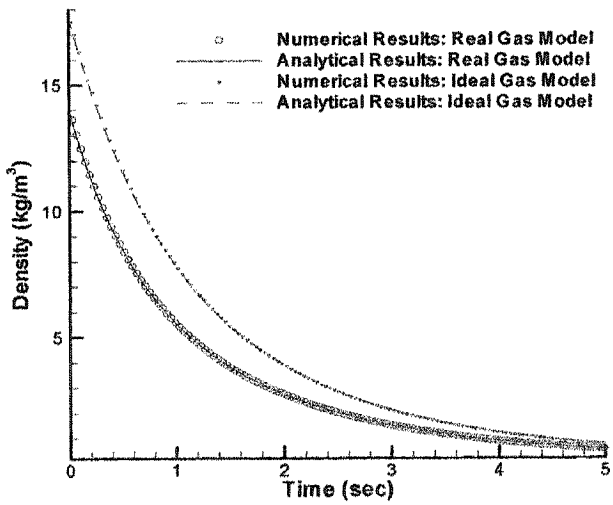

Fig. 4.4: *Analytical and numerical simulations of the flow density at the throat as a function of time for real and ideal gas conditions; hydrogen is released from a reservoir at initial pressure and temperature of 34.5 MPa and 300 °K.*

A lower critical pressure at the throat for real gas condition accompanies a lower critical temperature and density, as compared to the ideal gas flow behavior at the throat, fig. (4.3) and (4.4).

The stagnation pressure, temperature and density of the gas inside the chamber are shown in figs. (4.5) to (4.7). Similar to the sonic properties, comparisons have been done between analytical and numerical predictions for real and ideal gas conditions. A maximum error of 1% exists between the analytical and the numerical simulations for both the real and the ideal gas models. The relative error has its maximum value at the end of the release simulation.

For real gas model, pressure, temperature and density decay more rapidly than those for ideal gas model. The initial higher flow velocity at the throat, results in higher amounts of mass and energy out-fluxes for real gas model, which in turn lead to rapid decays of stagnation pressure, temperature and density.

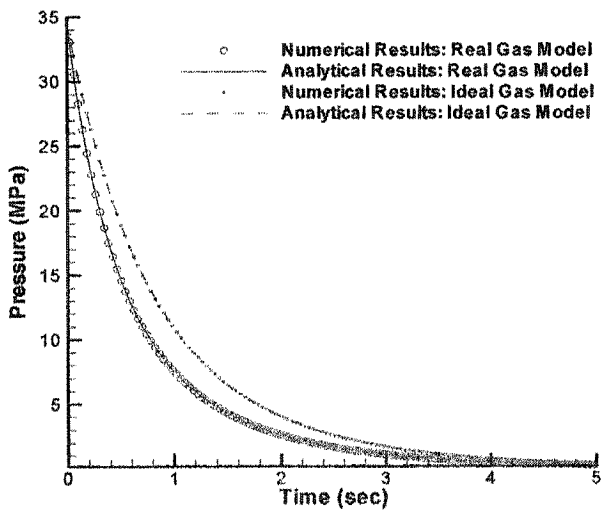

Fig. 4.5: *Analytical and numerical simulations of stagnation pressure inside the chamber as a function of time for real and ideal gas conditions; hydrogen is released from a reservoir at initial pressure and temperature of 34.5 MPa and 300 °K.*

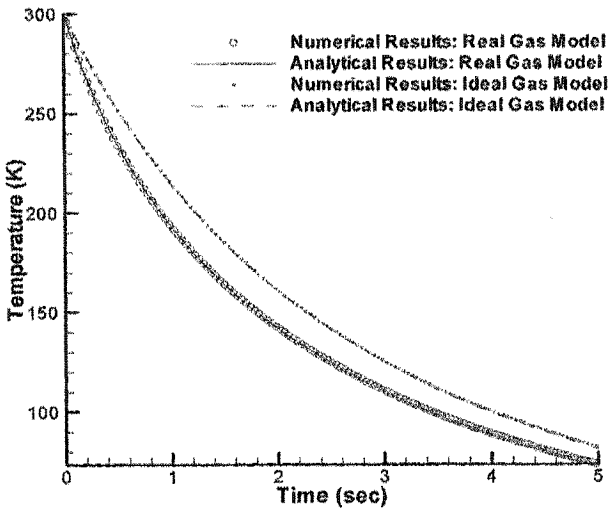

Fig. 4.6: *Analytical and numerical simulations of stagnation temperature inside the chamber as a function of time for real and ideal gas conditions; hydrogen is released from a reservoir at initial pressure and temperature of 34.5 MPa and 300 °K.*

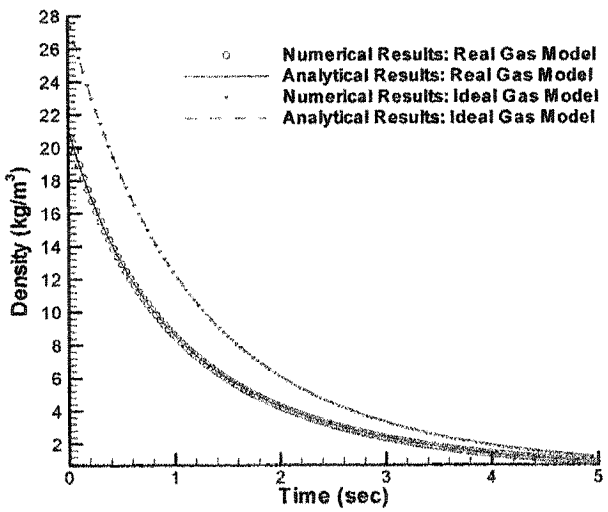

Fig. 4.7: *Analytical and numerical simulations of stagnation density inside the chamber as a function of time for real and ideal gas conditions; hydrogen is released from a reservoir at initial pressure and temperature of 34.5 MPa and 300 °K.*

A colder and less pressurized stagnant gas isentropically expands to lower sonic velocities at the throat. As shown in fig. (4.1), the flow velocity at the throat for real gas model is higher than the corresponding values for ideal gas model at the initial moments of the release when both ideal and real gases are expanding from approximately the same stagnation pressures and temperatures, figs. (4.5) to (4.7). After these initial moments, when the real gas is expanding from significantly lower stagnation pressures and temperatures, the throat velocity predicted by the real gas model decreases and becomes less than the values predicted by the ideal gas model. The foregoing trend of the sonic velocity affects the relative behavior of time histories of stagnation pressure, temperature and density for real and ideal gas models, figs. (4.5) to (4.7). The curves of the real and ideal gas models are diverging from each other at the beginning of the release. The divergence rate decreases and curves start converging when the sonic velocity for real gas model becomes less than the corresponding velocity for ideal gas model.

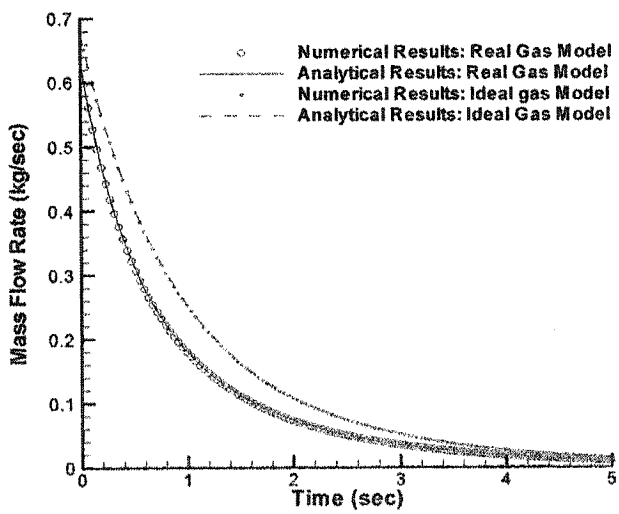

Fig. 4.8: *Analytical and numerical simulations of the mass flow rate exiting the chamber for real and ideal gas models as a function of time; hydrogen is released from a reservoir at initial pressure and temperature of 34.5 MPa and 300 °K.*

The time history of the mass flow rate exiting the chamber is shown in fig. (4.8), where the simulations for ideal and real conditions are performed based on the same initial total pressures and temperatures. The density predicted by ideal gas law is larger than the density real gas law predicts, fig. 1.1. Therefore, for ideal gas condition, the chamber contains more mass of hydrogen than that for real gas condition. Although the sonic velocity for real gas condition is higher than the corresponding value for ideal gas condition, the high-density hydrogen flow predicted by the ideal gas model results in a greater mass flow rate through out the release process. The time-integral of the mass flow rate (the area between the curve of the mass flow rate and the time axis) represents the total mass released from the chamber. The bigger area belongs to the ideal gas simulation.

Fig. 4.9 shows the mass flow rate exiting the chamber for ideal and the real gas conditions obtained from the numerical simulations when the total mass inside the chamber and the initial temperature are kept constant. The mass flow rates for real and ideal conditions follow the same pattern as that of the sonic velocity. At the beginning of the release the prediction of the real gas model is 20% greater than the ideal values.

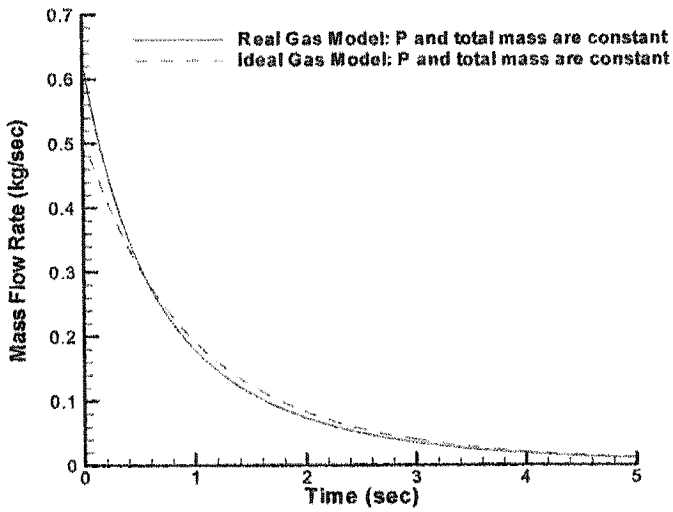

Fig. 4.9: *Analytical and numerical simulations of the mass flow rate exiting the chamber for real and ideal gas models as a function of time; hydrogen is released from a reservoir at initial pressure and temperature of 34.5 MPa and 300 °K.*

Real gas effects are investigated in the adiabatic release of hydrogen from a high-pressure chamber. The analytical and numerical simulations are in a very good agreement with each other. The maximum relative error is less than 2%. The real gas behavior at high pressures results in 14% and 20% increases, respectively in the throat sonic velocity and the mass flow rate at initial moments of the release. Stagnation and sonic pressures and temperatures for real gas condition are less than the corresponding ideal values throughout the release. The reduced stagnation pressure and temperature slow down the initially higher sonic velocity and mass flow rate to lower values, as compared to the predictions of the ideal gas model.

Chapter 5

CONCLUSIONS AND RECOMMENDATIONS

5.1 Conclusions

Hydrogen release from a high-pressure chamber is simulated using both an analytical and a numerical method. The following remarks are made:

- An analytical model is developed based on the Beattie-Bridgeman EOS to simulate the hydrogen release from a high-pressure plenum;
- An existing Euler solver is modified, and Jacobians, eigenvectors, and transformation matrices are calculated based on the Beattie-Bridgeman EOS;
- Free-slip and supersonic-outlet boundary conditions are modified and applied to the simulation of real gas flows;
- The analytical and numerical results are in a very good agreement with each other. The maximum relative error is less than 2% for the model problem;
- The real gas behavior at high pressures results in 14% and 20% increases in the sonic velocity at the throat and the mass flow rate exiting the chamber, respectively, at the initial moment of the release;
- The stagnation and sonic pressure, temperature and density predicted by the real gas model are less than the corresponding ideal values throughout the release;
- The reduced stagnation pressure, temperature and density, slow down the initially higher sonic velocity and mass flow rate to lower values, as compared to the ideal gas predictions for the rest of the release;

- The simulation of hydrogen release from a high pressure chamber requires a substantially higher amount of CPU time compared to a similar simulation performed for the air release;
- No CFL instability restriction has been observed when the Jacobians and fluxes at the supersonic outlet boundary were evaluated based on the corresponding node values without any extrapolation;
- For ideal gas behavior, the in house finite volume code is approximately three times faster than the commercial FLUENT code to simulate hydrogen release from a high-pressure chamber;
- The in house finite volume code is a general simulation tool and can be applied to simulate the real gas flows for different geometries.

5.2 Recommendations

Following Recommendation may be useful for future work:

- The simulation can be performed based on a more specific EOS for hydrogen. Beattie-Bridgeman equation is a general EOS, which can be applied to different gasses by changing the coefficients of the equation. In order to obtain a more accurate simulation, a more specific EOS should be applied to model the real gas behaviors for hydrogen;
- Developing a parallel version of the in house finite-volume code can speed up the simulation process. By the use of a parallel code, we can avoid some limitations, which currently exist in terms of the memory and simulation time;

- An appropriate preconditioner can accelerate the simulation process by reducing the number of iterations required to solve equation (3.6);
- In order to simulate the flow of a mixture of real gases that are in thermochemical equilibrium, an appropriate EOS should be applied. Jacobians, eigenvectors and Roe's method should be modified according to this EOS, which takes into account the chemical reactions between different species;
- The existing in house finite-volume code can be applied to simulate the real gas flow for different geometries. The code currently has subroutines to treat free-slip, supersonic-outlet, and free-stream boundary conditions. New types of boundary condition may be needed to simulate the flow for different geometries;
- The in house finite volume code can be applied to design the valves required for hydrogen supply;
- The code can be modified to take into account the viscosity effects, which become important for the flow of a real gas in long ducts.

BIBLIOGRAPHY

[1] Wallace, J. S., *A Comparison of Compressed Hydrogen and CNG Storage*, International Journal Hydrogen Energy **9**(7): 609-611, 1984.

[2] Wallace, J. S., Ward, C. A., *Hydrogen as a Fuel*, International Journal Hydrogen Energy **8**(4): 255-268, 1983.

[3] Schmidt, D., Krause, U., Schmidtchen, U., *Nnumerical Simulation of Hydrogen Gas Release Between Buildings*, International Journal Hydrogen Energy **24**: 479-488, 1999.

[4] FLUENT 6 Documentation, "FLUENT.INC\fluent6.0\help\index.htm",Fluent Inc., 2001.

[5] Grossman, B., Walters, W. R., *An Analysis of Flux-Split Algorithm for Euler's Equations with Real Gases*, AIAA Journal **27**(5): 524-531, 1989.

[6] Grossman, B., Walters, W. R., *Flux-Split Algorithms for the Multi-Dimensional Euler Equations with Real Gases*, Computers & Fluids **17**(1): 99-112, 1989.

[7] Tannehill, J. C., Buelow, P. E., Ievalts, J. O., Lawrence, S. L., *Three Dimensional Upwind Parabolized Navier-Stokes Code for Real Gas flows*, Journal of Spacecraft and Rockets **27**(2): 150-159, 1990.

[8] Glaister, P., *An Approximate Linearized Riemann Solver for the Euler Equations for Real Gases*, Journal of Computational Physics **74**: 382-408, 1988.

[9] Vinokur, M., Montagne, J. L. *Generalized Flux-Vector Splitting and Roe Average for an Equilibrium Real Gas*, Journal of Computational Physics **89**: 276-300, 1990.

[10] Liou M. S., Van Leer, B., Shuen, J. S., *Splitting of Inviscid Fluxes for Real Gases*, Journal of Computational Physics **87**: 1-24, 1990.

[11] Abgrall, R., *An Extension of Roe's Upwind Scheme to Algebraic Equilibrium Real Gas Models*, Computers & Fluids **19**(2): 171-182, 1991.

[12] Toumi, I., *A Weak Formulation of Roe's Approximate Riemann Solver*, Journal of Computational Physics **102**: 360-373, 1992.

[13] Buffard T., Gallouet T., Herard, J. M., *A Sequel to a Rough Godunov Scheme: Application to Real Gases*, Computers & Fluids **29**: 813-847, 2000.

[14] Mottura, L., Vigevano, L., Zaccanti, M., *An Evaluation of Roe's Scheme Generalizations for Equilibrium real Gas Flows*, Journal of Computational Physics **138**: 354-399, 1997.

[15] Johnson, R. C., *Real-Gas Effects in Critical Flow through Nozzles and Thermodynamic properties of Nitrogen and helium at pressures to 300 bar*, Lewis Research Center, Cleveland, Ohio, NASA SP-3046, 1968.

[16] Johnson, R. C., *Real-Gas Effects in Flow Metering*, Technical paper-Society of Manufacturing Engineers: 269-278, 1974.

[17] Saad M., *Compressible Fluid Flow*, 2nd ed. Englewood Cliffs, New Jersey: Prentice-Hall, 1985.

[18] Van Wylen, G. J., Sonntag, R. E., *Fundamental of classical thermodynamics*, 2nd ed., New York: John Wiley & Sons, 1976.

[19] *Journal of Physical and Chemical Reference Data: NIST-JANNAF Thermochemical Tables*, 4th ed., New York, New York: American Chemical Society and American Institute of Physics, 1998.

[20] Chapra, S. C., Canale, R. P., *Numerical Methods for Engineers*, 4th ed., New York: McGraw-Hill, 2002.

[21] Xu, T., *A study of an ILU preconditioned multi-model formulation for compressible flows*, M.A.Sc. Thesis, University of Toronto, Toronto, 2002.

[22] Hirsch, C., *Numerical computation of internal and external flows*, Vol. 2, New York: John Wiley & Sons, 1992.

[23] Peyret, R., *Handbook of Computational Fluid Mechanics*, London: Academic Press, 2000.

[24] Leveque, R. J., *Finite Volume Methods for Hyperbolic Problems*, Cambridge: Cambridge University Press, 2002.

[25] Apostol, T. M., *Linear Algebra: A First Course, with Application to Differential Equations*, New York: Wiley, 1997.

[26] Saad, Y., Schultz M. H., *A Generalized minimal Residual Algorithm for Solving Nonsymmetric Linear Systems*, SIAM Journal of Scientific Computation **7**: 856-869, 1986.

[27] Smith, R. G., *Efficient Construction and Utilization of Approximate Riemann Solutions*, Transaction of the American Mathematical Society **249**(1): 1979.

[28] Montagne, J. L., Yee, H. C., Vinokur, M., *Comparative Study of High-Resolution Shock Capturing Schemes for a Real Gas*, AIAA Journal **27**(10): 1332-1346, 1989.

[29] Tannehill, J. C., Lawrence, S. L., *Upwind Parabolized Navier Stokes Code for Chemically Reacting Flows*, Journal of Thermophysics and Heat Transfer, 4(2): 149-156, 1990.

[30] GAMBIT 2.0.4. Documentation, "FLUENT.INC\fluent6.0\help\index.htm", Fluent Inc., 2001.

Appendix A

SPECIFIC HEATS OF HYDROGEN AT CONSTANT PRESSURE, [19]

T °K	C_P J·(kg °K)$^{-1}$	T °K	C_P J·(kg °K)$^{-1}$
0	0	2900	1882.8
100	13966.1	3000	18397.4
200	13615.4	3100	18508.5
250	14060.4	3200	18616.2
298.15	14304.4	3300	18721.4
300	14310.9	3400	18823.5
350	14426	3500	18924.2
400	14475.6	3600	19023
450	14499.4	3700	19120.2
500	14514.8	3800	19216.4
600	14548	3900	19310.7
700	14604.5	4000	19403.9
800	14695.3	4100	19495.7
900	14822.8	4200	19586.5
1000	14983.5	4300	19676.3
1100	15170	4400	19764.1
1200	15373.9	4500	19850.9
1300	15587.7	4600	19935.7
1400	15805	4700	20018.6
1500	16021.8	4800	20099.4
1600	16233.6	4900	20177.8
1700	16439	5000	20253.7
1800	16636.4	5100	20326.6
1900	16824.9	5200	20396.6
2000	17005	5300	20463.5
2100	17175.6	5400	20526.5
2200	17338.3	5500	20585.6
2300	17492.6	5600	20640.6
2400	17639.4	5700	20691.7
2500	17779.8	5800	20738.3
2600	17913.3	5900	20780
2700	18041.7	6000	20817.2
2800	18164.8		

Appendix B

ENERGY EQUATION IN TERMS OF PRESSURE

The conservation equations are recast to a final form in terms of the primitive variables. This form is appropriate to calculate the primitive Jacobian matrices, Section 3.4.2.

We start by rewriting the conservation equations given in equations (3.52):

$$\frac{\partial \rho}{\partial t} + \left(\vec{V} \cdot \vec{\nabla} \rho\right) + \rho \vec{\nabla} \cdot \vec{V} = 0, \tag{B.1}$$

$$\frac{\partial \vec{V}}{\partial t} + \left(\vec{V} \cdot \vec{\nabla}\right)\vec{V} + \frac{\vec{\nabla} P}{\rho} = 0, \tag{B.2}$$

$$\frac{\partial E}{\partial t} + \left(\vec{V} \cdot \vec{\nabla}\right)E + \frac{1}{\rho}\vec{\nabla} \cdot \left(\vec{V} P\right) = 0. \tag{B.3}$$

The objective is to transform equation (B.3) to an equation for pressure. First, we obtain a relation for the isentropic pressure derivative of internal energy. The following relations exist between the change in enthalpy and internal energy of a pure substance, [18]:

$$Tds = dh - \frac{dP}{\rho} = di + pd\left(\frac{1}{\rho}\right). \tag{B.4}$$

In an isentropic process, (B.4) can be written as:

$$dh - \frac{dP}{\rho} = di + pd\left(\frac{1}{\rho}\right) = 0. \tag{B.5}$$

Therefore, we have,

$$\left(\frac{\partial h}{\partial P}\right)_s = \frac{1}{\rho}, \tag{B.6}$$

and

$$\left(\frac{\partial i}{\partial P}\right)_s = \left(\frac{\partial h}{\partial P}\right)_s - \frac{1}{\rho} + \frac{P}{\rho^2}\left(\frac{\partial \rho}{\partial P}\right)_s. \tag{B.7}$$

Substituting equation (B.6) and the definition of sound velocity given by equation (2.18) into equation (B.7), we have,

$$\left(\frac{\partial i}{\partial P}\right)_s = \frac{P}{\rho^2 a^2}. \tag{B.8}$$

Second, we obtain the final from of equation (B.3). The scalar product of the momentum equation (B.2) by the velocity vector $\vec{V}$ can be written as:

$$\frac{\partial}{\partial t}\left(\frac{V^2}{2}\right) + \left(\vec{V}\cdot\vec{\nabla}\right)\frac{V^2}{2} + \frac{\vec{\nabla}P\cdot\vec{V}}{\rho} = 0. \tag{B.9}$$

Equation (B.3) can be expanded to the following form:

$$\frac{\partial i}{\partial t} + \frac{\partial}{\partial t}\left(\frac{V^2}{2}\right) + \left(\vec{V}\cdot\vec{\nabla}\right)i + \left(\vec{V}\cdot\vec{\nabla}\right)\frac{V^2}{2} + \frac{P}{\rho}\left(\vec{\nabla}\cdot\vec{V}\right) + \frac{\vec{\nabla}P\cdot\vec{V}}{\rho} = 0. \tag{B.10}$$

Subtracting equation (B.10) from equation (B.9), we have

$$\frac{\partial i}{\partial t} + \left(\vec{V}\cdot\vec{\nabla}\right)i + \frac{P}{\rho}\left(\vec{\nabla}\cdot\vec{V}\right) = 0. \tag{B.11}$$

The derivatives of internal energy can be replaced with the derivatives of pressure from equation (B.8),

$$\frac{\partial P}{\partial t} + \left(\vec{V}\cdot\vec{\nabla}\right)P + \rho a^2\left(\vec{\nabla}\cdot\vec{V}\right) = 0. \tag{B.12}$$

Equation (B.12) is the equivalent form of the conservation of energy, which is given in terms of pressure.